NATIONAL ADVISORY COMMITTEE FOR AERONAUTICS

TECHNICAL NOTE 4286

MECHANISM OF BENEFICIAL EFFECTS OF BORON AND ZIRCONIUM ON CREEP-RUPTURE PROPERTIES OF A COMPLEX HEAT-RESISTANT ALLOY

By R. F. Decker and J. W. Freeman
University of Michigan

Washington
August 1958

NATIONAL ADVISORY COMMITTEE FOR AERONAUTICS

TECHNICAL NOTE 4286

MECHANISM OF BENEFICIAL EFFECTS OF BORON AND ZIRCONIUM ON CREEP-RUPTURE PROPERTIES OF A COMPLEX HEAT-RESISTANT ALLOY

By R. F. Decker and J. W. Freeman

SUMMARY

The mechanism by which the addition of boron and zirconium improves the creep-rupture properties of an alloy of 55 percent nickel, 20 percent chromium, 15 percent cobalt, 4 percent molybdenum, 3 percent titanium, and 3 percent aluminum was investigated at 1,600° F. Materials with varying boron and zirconium content were exposed to creep conditions, and then the microstructures were analyzed by optical and electron microscopy, electron diffraction, microfractography, and hardness measurements. Interrupted creep tests that allowed comparisons of materials after equivalent creep exposures were particularly useful.

The creep-rupture properties were improved because the boron and zirconium have a pronounced stabilizing effect on the grain boundaries of the alloy. The alloy with low boron and zirconium content was subject to rapid agglomeration of $M_{23}C_6$ and γ' in the grain boundaries, followed by depletion of γ' and intergranular micro-cracking at the grain boundaries transverse to applied stress. Brittle fracture then occurred by linking of micro-cracks. However, additions of zirconium, boron, or boron plus zirconium decreased this tendency in that order. In the absence of these elements extensive micro-cracking was found early in second-stage creep at relatively short time periods, and fracture occurred prematurely with very little deformation. Proper amounts of boron plus zirconium delayed micro-cracking until after third-stage creep started, so that creep-rupture life was greatly prolonged and ductility to fracture was markedly increased.

No effect of the trace elements on the size, amount, and distribution of the intragranular γ' was detected. Thus, the property effects did not result from a change in the intragranular γ' reaction.

The significant structural features were evident only after limited amounts of creep. The damaging structural changes are apparently

comparable at fracture for material with varying amounts of trace elements, even though the rupture time and ductility vary greatly for material tested at a common stress. The generality and limitations of the mechanism are estimated.

INTRODUCTION

Recent investigations have revealed the importance of trace boron and zirconium in determining the creep-rupture properties of heat-resistant nickel-base alloys. This study is concerned with the mechanism of the effects of adding boron or zirconium, or both, to these alloys.

A recent study (ref. 1) of effects of variable melting practice on heat-to-heat variations in properties of a nickel-base alloy (55% Ni, 20% Cr, 15% Co, 4% Mo, 3% Ti, 3% Al) indicated that introducing a trace of boron or zirconium inadvertently from crucible contamination or purposely in deoxidation was the most important melting practice variable. As a result of this practice, the following facts have been determined:

(1) Creep-rupture life and ductility at 1,600° F and 25,000 psi increased with boron content when zirconium was less than 0.01 percent (fig. 1).

(2) Creep-rupture life and ductility at 1,600° F and 25,000 psi increased with zirconium content when boron was less than 0.0005 percent (fig. 2).

(3) The addition of 0.01 percent zirconium to material containing 0.009 percent boron raised both creep-rupture life and ductility significantly above those of the material with either element alone.

(4) Minimum second-stage creep rates were lowered slightly by the addition of zirconium and more markedly by boron (fig. 3).

Reference 2 shows benefits to both creep-rupture life and ductility of M-252, Udimet 500, Inco 700, Nimonic 90, and Waspaloy alloys from boron and zirconium addition. Confirmation of the effects of boron on commercial nickel-base alloys is presented in reference 3. The effects are not wholly restricted to the nickel-base alloys, however. The creep-rupture properties of other alloy systems have also been improved.

Since the helpful effects of boron and zirconium on creep-rupture properties are found in many alloy systems, establishing the mechanism for the effects is desirable. Such a mechanistic approach should increase knowledge in theory of alloying and give a more basic understanding of alloy design to resist creep. In addition, such a study might also reveal the nature and cause of rupture in these materials.

Therefore, an investigation was undertaken to establish the mechanism for the beneficial effects of boron and zirconium on the creep-rupture properties of a heat-resistant nickel-base alloy. The experimental procedure consisted in studying the microstructures. A material composed of 55 percent nickel, 20 percent chromium, 15 percent cobalt, 4 percent molybdenum, 3 percent titanium, and 3 percent aluminum was selected because the effects were established on this composition and because stock with established creep-rupture properties and chemistry was available.

It is generally accepted that the favorable high-temperature properties of the titanium-aluminum-hardened nickel-base alloys result from the precipitation of the intermetallic γ' phase within the matrix of the alloy. The γ' phase has been shown to have a face-centered cubic structure similar to that of the Ni_3Al phase of the nickel-aluminum system with a lattice parameter closely matched to that of the matrix of the alloys (refs. 4 and 5). Compositionally, the phase has been shown to dissolve titanium and is frequently referred to as $Ni_3(Al,Ti)$.

The creep resistance of these alloys has been attributed to the presence of γ' (refs. 4 and 6) and to the fact that γ' forms in fine dispersion within the matrix; however, attempts to relate the distribution of the γ' particles with the metallurgical properties have been only moderately successful to date. Reference 7, and subsequently reference 8, showed that dispersion of the γ' particles in Inconel-X alloy correlated with creep-rupture properties at 1,200° F, which was low in the aging range for this alloy; however, no correlation was obtained for rupture tests at 1,500° F, which was high in the aging range. In reference 9 the relations between structure and creep properties were studied for several Nimonic alloys tested high in the aging range. Highest creep-rupture properties were obtained with the greatest volume-percent of γ'. Reference 10 found that the best creep resistance in nickel-chromium-aluminum-titanium alloys was obtained with the highest density of γ' particles as counted in electron micrographs.

Carbide reactions occur in the titanium-aluminum-hardened nickel-base alloys and have been related to properties. Among the carbides identified are $M_{23}C_6$ (refs. 8, 11, and 12), M_6C (refs. 11 and 12), Cr_7C_3 (ref. 13), and TiC (refs. 11 and 12). The occurrence of a particular type of carbide depends both on the alloy content and on the temperature of treatment. In general, the carbide reactions in these alloys are poorly understood. Their probable importance in controlling properties is indicated in reference 13, which establishes the benefits on rupture life of obtaining a high-temperature precipitate of Cr_7C_3 before creep exposure of Nimonic alloys. Judging from the moderate success of previous work in relating the γ' and carbide reactions to properties, it is

logical that the effect of trace elements on the alloy is the modification of these property-controlling reactions.

This investigation was conducted at the University of Michigan under the sponsorship and with the financial assistance of the National Advisory Committee for Aeronautics. The chemical analyses were supplied gratis by Utica Drop Forge and Tool Division of Kelsey-Hayes Co. and Universal-Cyclops Steel Corp. Particular credit is due Dr. W. C. Bigelow and Mr. J. A. Amy for the phase identifications, which were part of a program of research in identification of minor phases in heat-resistant alloys sponsored by Metallurgy Research Branch, Aeronautical Research Laboratory, Wright Air Development Center. The technical advice of Professors Thomassen, Flinn, and Brockway and Mr. J. P. Rowe was very helpful. Invaluable assistance in the experimental program was provided by A. Dano, K. Kienholz, T. Cullen, G. Hynes, D. Umstead, and C. Sadler.

EXPERIMENTAL PROCEDURES

The general procedure was to observe microstructural changes when materials with varying boron and zirconium content were subjected to thermal treatments involving temperature and stress.

Material

The experimental heats of the alloy (55% Ni, 20% Cr, 15% Co, 4% Mo, 3% Ti, 3% Al) were induction-melted in the University of Michigan vacuum-melting furnace. The virgin melting stock was composed of electrolytic nickel, electrolytic chromium, electrolytic cobalt, arc-melted molybdenum, Ti 55A titanium, 99.99-percent-aluminum pig, electrolytic manganese, 99.9-percent-silicon powder, and spectrographically pure carbon. Boron was added to heats V + B and V + B + Zr as NiB. The zirconium contained in heats V + Zr and V + B + Zr was derived from reaction with zirconia crucibles used in melting. Heat V was melted in an alumina crucible, and heat V + B was melted in a magnesia crucible.

The 10-pound ingots were processed as follows: (1) homogenized 1 hour at 2,300° F and air-cooled; (2) surface ground; and (3) rolled to 7/8-inch bar stock from 2,150° F. Twenty-two passes, each of about 7-percent reduction in area, were used with 10-minute reheats at 2,150° F between passes. Sections of the bar stock that originally were at the ingot center were chemically analyzed. In addition, material after creep exposure was tested for boron content. The results are listed in table I. Boron and zirconium were determined to be the significant heat-to-heat variables. The heats are coded to indicate the relative boron and zirconium level - heat V having low boron and zirconium content, heat V + Zr

having relatively high zirconium content, heat V + B having relatively high boron content, and heat V + B + Zr having significant content of both boron and zirconium. All the stock was homogenized 2 hours at 2,150° F and air-cooled before further experimentation.

Stress-Aging and Stress-Rupture Testing

Treatments under stress were performed in stress-rupture units; strain was measured with an extensometer-mirror system with a sensitivity of 0.000005 inch per inch.

Solution-treated bar stock was machined to 0.250-inch test specimens with a 1-inch-gage section. A uniform time period of 4 hours of preheating at test temperature in the stress-rupture units was used before stress application. The stress-aged samples were interrupted at the desired time by release of the load and immediate removal from the furnace.

Hardness

Diamond pyramid hardness (DPH) was measured with a 50-kilogram load. Three impressions were made on each sample, both diagonals of each impression being measured. Statistical analysis of testing variability established that in the range of 200 to 340 DPH a hardness difference of 7 DPH was significant, while in the range of 340 to 400 DPH a hardness difference of 9 DPH was significant.

Metallography

Light microscopy. - The metallographic samples for light microscopy were mechanically polished through wet papers to 600 grit. Most of the samples were then polished on wet cloths with Linde A and Linde B powders; a few, as noted in the figures, were electropolished in a solution of 10 parts of perchloric acid (70 percent) and 90 parts of glacial acetic acid at 50 volts with a current density of 2 amperes per square inch. Cyclic polishing of 5 seconds on and 5 seconds off was employed for a total period of electrolysis of 30 seconds.

The procedure and etchant developed by the authors of reference 14 were used to reveal best the precipitating phases at 100, 1,000, and 2,000 diameters. Etching was electrolytic at 6 volts and a current density of 0.8 ampere per square inch for periods of 5 to 7 seconds, depending upon the sample condition. The etchant was composed of 12 parts of phosphoric acid (85 percent), 47 parts of sulfuric acid (96 percent), and 41 parts of nitric acid (70 percent).

Electron microscopy. - The metallographic samples for electron microscopy were mechanically polished through wet papers to 600 grit and electropolished in the same way as the samples for light microscopy. Etching for the electron microstructures was accomplished with the etchant described for light microscopy using 6 volts and a current density of 0.8 ampere per square inch for periods of 1 to 5 seconds.

After etching, collodion replicas of the metallic surface were made. These were shadowed with palladium to increase contrast and reveal surface contours; polystyrene latex spheres approximately 3,400 angstroms in diameter were placed on the replicas prior to shadowing to indicate the angle and direction of shadowing and to provide an internal standard for measurement of magnification. The micrographs reproduced in this paper are copies of direct prints from the original negatives; consequently, the polystyrene spheres appear black and the "shadows" formed by the palladium appear white.

Counting techniques. - Depleted grain boundaries, micro-cracks, nodules, and surface cracks were detected in this study. In order to make the trends and comparisons quantitative, counts were made of the number of each feature in the area traversed. The depleted grain boundaries, micro-cracks, and nodules were surveyed on mechanically polished and etched specimens with an oil-immersion lens at a magnification of 1,000 diameters. An area of 0.008 square inch, composed of eight strips, each 0.2 by 0.005 inch, was covered. In the interrupted creep tests, the strips were longitudinal to the specimen axis at the center of the specimen and at the minimum cross section. In ruptured samples, the strips were again longitudinal, starting in the grains at the fracture surface and progressing away from the fracture. A depleted grain boundary was counted when a clear, white strip of matrix free of γ' particles was clearly seen along a grain boundary. Micro-cracks were easily distinguishable by their blackness, which contrasted with all other intragranular and intergranular features of the samples. Early doubts about the identity of these cracks were eliminated when electropolishing enlarged and accentuated these black voids and when fins on electron microscope replicas were found where the micro-cracks had been filled. Each distinct micro-crack was counted; 1 micron was selected as the minimum size counted, since shorter micro-cracks were not distinguishable from carbide-matrix interfaces. Counting of nodules was arbitrarily limited to those above 5 microns in diameter.

Intergranular surface cracks were counted on mechanically polished creep specimens by traversing longitudinal section surfaces at a magnification of 500 diameters. This cracking was quite uniform over the reduced section of the specimens. In the interrupted creep specimens the cracks were counted over the center 0.75 inch, while in ruptured samples counts were made for 0.50 inch from the fracture. Intergranular cracks penetrating more than 0.003 inch deep were counted.

A rough measure of γ' dispersion was obtained by the surface density of γ' particles in electron microstructures. An area large enough to contain at least 100 particles was surveyed at 12,000 diameters.

These techniques allow quantitative comparison of the tendency of the four heats to undergo the changes. It is recognized that percentage of grain-boundary area cracked, percentage of grain-boundary area depleted, volume-percent of nodules, and volume-percent and interparticle distance of γ' would be fundamentally more sound quantities for correlation. However, these more refined and time-consuming techniques would not alter the conclusions of this paper and therefore were not considered necessary.

4935

Electron Diffraction

The extraction-replica technique of reference 15 was used to permit identification of precipitating phases by electron diffraction.

Specimen preparation. - For extraction of intragranular γ', the specimens were electropolished and etched as they were for electron microscopy. The specimen preparation for extraction of intragranular carbides consisted in electropolishing and then immersion-etching for 5 seconds in aqua regia in order to remove γ'.

For extraction of intergranular particles, the microfractographic techniques of reference 16 proved very useful. Specimens were cooled in liquid nitrogen and then fractured with a hammer and chisel, the fracture being intercrystalline. The fracture surface was then etched by the same procedure described for extraction of intragranular carbides.

Replication. - Carbon replica films were deposited on the prepared surfaces by the method of reference 17 and were backed by thicker supporting films of collodion. The surfaces were then etched electrolytically in a solution of 2 parts phosphoric acid (85 percent) to 8 parts water until the compound replica films separated from them. The films were transferred to the surface of clean distilled water and allowed to wash by diffusion. They were then picked up on nickel screens and washed again, and the collodion backing films were dissolved from the carbon films with amyl acetate by the method of reference 18. The replicas were then shadowed with aluminum to provide an internal standard for interplanar distances. Electron micrographs were obtained from the replicas in an RCA Model EML electron microscope. In addition, electron diffraction patterns were obtained from the particles by selected area electron diffraction techniques on the microscope.

Thermal Exposures Used Before Microstructural Examination

The four experimental heats were exposed to several treatments before microstructural examination. The exposures, purpose of each, and limitations on comparison were as follows:

(1) No exposure, initial condition as solution-treated 2 hours at 2,150° F and air-cooled; to detect differences in microstructure before creep exposure

(2) Aged 1/2, 1, 4, 10, 100, 188, and 500 hours at 1,600° F; to show response of materials to temperature effects alone

(3) Stress-aged 165 hours at 1,600° F and 20,000 psi; to show response to creep exposures of equal stress and time (because of differing creep rates, as shown in fig. 4(a), total creep deformations were unequal)

(4) Stress-aged to rupture at 1,600° F and 25,000 psi; to show response to creep exposures of equal stress (because of varying rupture life and ductility, as shown in fig. 4(b), exposure times and total creep deformations were unequal)

(5) Stress-aged at 1,600° F at stresses selected to give comparable time-elongation curves; to compare response to creep exposures of equal strain, strain rate, and time (because of varying creep rates, stresses were unequal: Heat V, 20,000 psi; Heat V + Zr, 22,500 psi; Heat V + B, 28,000 psi; Heat V + B + Zr, 30,000 psi)

Rupture times for those stress-aged samples which were run to rupture are plotted in figure 5. Data on stress-aging are listed in table II.

RESULTS

Marked microstructural changes occurred in heat V during creep exposure at 1,600° F. In terms of properties, the most significant changes were at the grain boundaries, where a process of agglomeration of $M_{23}C_6$, depletion of γ' precipitates, micro-cracking, and finally brittle fracture occurred. This process was retarded by the addition of zirconium, more by boron, and most by boron with zirconium.

Other microstructural features developed during exposure at 1,600° F, including intragranular M_6C in the heats with boron, alinement of γ', intergranular surface cracking, and nodular mixtures of carbides and γ'. The details of the grain-boundary changes as well as other microstructural changes are given in the following sections.

The light micrographs presented are mounted with the rolling direction (and axis of tension in the case of creep specimens) vertical and in the plane of the figure. The orientation of electron micrographs was not determined except where noted in the figures.

Microstructures in Initial Condition

After the initial homogenizing treatment of 2 hours at 2,150° F and air-cooling, the experimental heats were similar in grain size (fig. 6(a)), inclusion count and distribution (fig. 6(a)), and grain-boundary precipitate (figs. 6(b) and (c)). The γ' precipitated during the air-cooling after the 2,150° F treatment. Some slight differences in dispersion of intragranular γ' existed, but these were not significant, as discussed later. Hardnesses (fig. 6(a)) did not differ significantly in this condition.

Changes in Microstructure During Exposure at 1,600° F

Tables III and IV list the quantitative data on microstructural changes.

Agglomeration in grain boundaries. - A network of carbides enveloped by γ' accumulated in the grain boundaries of all samples during exposure at 1,600° F. In heat V, the rate of accumulation was comparatively rapid, the carbide phase being extensive and massive and the γ' layer thick after 165-hour exposure with 1.2-percent creep deformation (fig. 7). The amount of agglomeration under these conditions was somewhat lower in heat V + Zr and much lower in heats V + B and V + B + Zr (figs. 7(b) and (c)).

The agglomerated γ' was easily identified by etching characteristics. The agglomerate reacted to etching in the same manner as the intragranular γ' in all the experimental work carried out. It was always in the same relief and had the same appearance as the intragranular γ'.

Microfractographic techniques were used to identify the carbide phase and to obtain more information on its form. Samples from heats V and V + B after 1.2-percent creep deformation at 1,600° F in 165 to 188 hours were cooled in liquid nitrogen and then fractured. Extraction replication from the fractured surface removed the grain-boundary carbide and retained it in the replica. Electron micrographs showing the size and distribution of carbides in the grain boundaries are shown in figure 8. The extracted particles from heat V were larger, more extensive, and thicker than those from heat V + B. The electron diffraction data obtained on the replicas of the two samples indicated $M_{23}C_6$.

Depletion of γ' at grain boundary. - Subsequent to the agglomeration of $M_{23}C_6$ in the grain boundaries, strips of matrix were depleted of γ' particles along transverse grain boundaries of the stress-aged specimens (fig. 9). This occurred most often adjacent to $M_{23}C_6$ particles. This was in contrast to samples aged without stress, where the intergranular $M_{23}C_6$ was always enveloped by γ' and where the fine γ' particles extended up to the grain boundary (fig. 10).

In figure 9, the amount of this depletion is related to creep deformation for the experimental heats exposed to give equal strain at equal time at 1,600° F. It is evident that boron and zirconium are effective in reducing the amount of this depletion with a given strain at 1,600° F. Since the samples were stressed to give comparable strain rates, it follows that depletion in a given time at 1,600° F was reduced. Despite this retarding influence, however, the amounts of depletion at fracture became comparable under influence of increased strain in heats V + Zr, V + B, and V + B + Zr.

In samples ruptured at 1,600° F and 25,000 psi (fig. 11), the depletion was extensive. Often, layers of precipitate-free matrix as thick as 5 to 10 microns were found. In this case, comparison of retardation was limited by the unequal exposure times and strains.

After 165 hours at 1,600° F at an equal stress of 20,000 psi, the retarding effect of boron and zirconium was even more evident. While 264 depleted boundaries were found in heat V, only 72 were found in heat V + Zr, 16 in heat V + B, and none in heat V + B + Zr (table III).

Micro-cracks. - Following agglomeration of $M_{23}C_6$ and depletion of γ' in the grain boundaries, micro-cracks appeared. These appeared as dark areas in mechanically polished samples (fig. 7(b)). Confirming evidence of these was found in electron microscopy, where the replicas contained fins where the collodion had filled micro-cracks and then had been extracted during stripping of the replica from the metal surface. The fins appeared black in the electron microstructures (fig. 7(c)), with white shadows from palladium.

The micro-cracks were associated with $M_{23}C_6$ particles in the grain boundaries transverse or nearly transverse to the applied stress, usually being at an $M_{23}C_6$-matrix interface or between tips of $M_{23}C_6$ particles. In either case cracks formed where depletion of γ' had occurred. Often, several separate micro-cracks were detected in one grain boundary with no preference being shown for triple points. These separate cracks seemed to link together with further creep exposure; this constituted the mode of fracture in heat V.

Figure 12 relates micro-cracking to creep deformation for the experimental heats exposed to give equal strain in equal time at 1,600° F. The number of cracks for a given creep strain or exposure time diminished in heat V + Zr, heat V + B, and heat V + B + Zr in that order. Five micro-cracks were detected in heat V at the end of first-stage creep, when only 15 percent of the rupture life was expended. In heat V + B + Zr, only two micro-cracks were found at 80 percent of the rupture life, when tertiary creep had already commenced. The amount of micro-cracking at fracture also diminished in the order heat V, heat V + Zr, heat V + B, and heat V + B + Zr. When the four heats were exposed 165 hours at 1,600° F and 20,000 psi, the difference in micro-cracking was even more pronounced. In heat V, 314 micro-cracks were counted; whereas only 9 were counted in heat V + Zr and none in heats V + B and V + B + Zr. It was evident from the specimens tested at 1,600° F and 25,000 psi that, although micro-cracking was retarded, it was not prevented by the addition of boron and zirconium (table III).

Intergranular surface cracking. - In addition to micro-cracks within the specimens, the heats were subject to intergranular cracking from the specimen surface during creep-rupture tests. Initiation of these cracks was definitely from the specimen surface, with a gradual increase in number and depth during creep exposure. Some of these cracks are pictured in figure 13, and quantitative data on amounts are listed. Figure 13(a) shows that the specimen of heat V run at 1,600° F and 25,000 psi had negligible surface cracking at the time of rupture, 52 hours. The mode of fracture was by linking of the interior micro-cracks evident in figure 13. However, in heat V + B run at 1,600° F and 28,000 psi, the amount of micro-cracking was diminished but surface cracking is evident (fig. 13(b)). The importance of these surface cracks in fracture is indicated by the sample from heat V + B + Zr run at 1,600° F and 30,000 psi, where some of the surface cracks penetrated more than 1/4 of the specimen radius (fig. 13(c)).

The quantitative data for surface cracks seems to indicate that the addition of trace elements modified the mode of fracture. Surface cracking increasingly competes with micro-cracking as a source of fracture when the tendency for micro-cracking is reduced.

Intragranular precipitation of carbide. - The boron-containing heats had less tendency to intergranular $M_{23}C_6$ but precipitated more carbide intragranularly during exposure at 1,600° F (fig. 7(c)). The form of this carbide depended on stress. Short plate-like carbides formed in samples aged without stress. In the stress-aged samples these were more elongated in form (compare figs. 7(b) and 10(a)) and had a tendency to precipitate on preferred matrix planes. As shown in figure 8(d), the carbides were extracted from heat V + B after 1.2-percent creep strain in 188 hours at 1,600° F. Most of the spots in the electron diffraction

pattern indicated the presence of M_6C, with some spots corresponding to $M_{23}C_6$. Therefore, it seemed that some of the intragranular carbide, if not all, was M_6C rather than $M_{23}C_6$.

The intragranular carbide was distributed fairly uniformly throughout the grains in the boron heats, with some concentration near the Ti(C,N) particles.

There was some evidence that intragranular carbides diminished and carbides increased in the grain boundaries during long time exposure, indicating that carbon was diffusing to the grain boundaries.

Intragranular γ'. - The intragranular precipitates of γ' grew and agglomerated during aging at 1,600° F. As measured by the surface density of γ' particles in electron micrographs, there was no significant effect of boron, zirconium, or stress on this reaction (fig. 14). Therefore, the differences in surface density of γ' existing after the 2,150° F treatment and air-cooling were not lasting and appeared to be unimportant.

As a further means of evaluating effects of trace elements on aging of γ' at 1,600° F, the change of hardness with aging time at 1,600° F was measured (fig. 15 and table IV). The hardness changes for the four experimental heats were very similar, except that heat V + B + Zr aged to a higher hardness and retained this advantage at 500 hours. All heats reached maximum hardness at 1,600° F at about 1 hour and then overaged at longer times. Electron micrographs typical of the alloy showing γ' density are included in figure 15.

Although creep strain did not affect the density of γ' particles, it did modify the distribution of particles. Creep strains within the grains resulted in some preferential agglomeration of γ' on the slip planes, as evidenced by an alinement of γ'. This was especially noticeable after high creep strain (fig. 11). The γ' phase was identified by electron diffraction (fig. 8(c)).

Nodular precipitate. - All the materials exhibited nodules to some extent after aging at 1,600° F (fig. 16 and tables III and IV). The nodules, which often were seen to envelop or abut on carbon-rich Ti(C,N), appeared to be mixed carbide and γ'. As shown in figure 16, their occurrence was definitely accelerated by strain, especially in heat V. Likewise, they were controlled by trace elements in that their formation was retarded by boron and zirconium.

Boron content after creep exposure. - A specimen from heat V + B was analyzed for boron content after rupture in 428 hours at 1,600° F and 25,000 psi. The cross section of the specimen was analyzed at 0.0090

percent boron. A surface layer approximately 0.010 inch deep contained 0.0079 percent boron. These compared with the analysis of 0.0089 percent boron obtained in the as-rolled bar stock.

DISCUSSION

The microstructural studies revealed the role of boron and zirconium in increasing creep-rupture life and ductility of an alloy containing 55 percent nickel, 20 percent chromium, 15 percent cobalt, 4 percent molybdenum, 3 percent titanium, and 3 percent aluminum.

In the absence of boron and zirconium, $M_{23}C_6$ and γ' rapidly formed a network in the grain boundaries of the alloy during creep at 1,600° F. This was followed by depletion of γ' precipitates in the metal adjacent to the transverse grain boundaries and early intergranular micro-cracking at the $M_{23}C_6$-depleted-zone interfaces. The micro-cracks grew, linked, and initiated brittle and premature failure. Boron and zirconium retarded this grain-boundary process, thereby allowing longer creep exposure and higher creep deformation before the fracture mechanism operated.

Additional experimental support for the mechanism is obtained by relating creep-rupture life (fig. 17) and ductility (fig. 18) at 1,600° F and 25,000 psi to the tendency of the experimental heats to undergo depletion of grain boundaries and micro-cracking during 1.2-percent creep deformation in 165 to 214 hours at 1,600° F. It is evident from the data that the increase in creep-rupture life and ductility from the addition of the trace elements results from retardation, but not prevention, of the grain-boundary mechanism of carbide formation, grain-boundary depletion, and micro-cracking. The specimens from all the experimental heats were similar in degree of grain-boundary agglomeration of carbides, γ' depletion, and micro-cracking after rupture at 1,600° F and 25,000 psi. However, both the time and deformation at which the grain-boundary effects occurred and initiated fracture were increased by boron and zirconium.

The finding of only retardation of micro-cracking by boron and zirconium does not imply that their beneficial effects are only temporary in nickel-base alloys. All available data indicate that the boron and zirconium materials are superior to those free of boron and zirconium even at low stresses and in long time exposure.

The chemical analyses on heat V + B after rupture-testing indicated that loss of boron from the sample during testing did not occur except possibly at the surface. De-boronization does not appear to be the cause of the eventual appearance of the grain-boundary changes in boron-bearing material.

Interpretation of Other Microstructural Changes

Several other features of the data require discussion.

Intragranular carbide precipitation. - Apparently the occurrence of intragranular carbide in the heats with boron was related to retardation of $M_{23}C_6$ agglomeration in the grain boundaries. In a sense, a redistribution of carbide was effected by boron. In the case of zirconium additions, suppression of the grain-boundary agglomeration was not acccompanied by intragranular carbides, possibly because of the weaker effect at the grain boundary.

The intragranular carbide in the boron heats may have had a direct effect on properties in addition to tying up carbon to retard $M_{23}C_6$ agglomeration in grain boundaries. The form of the precipitate after creep indicates that it is strain-induced and may lower creep rate in a manner proposed by reference 19. According to reference 19, resistance to creep is obtained by nucleation and growth of precipitates in dislocations, preventing further movement of the dislocations through the lattice. The reaction would resemble strain-aging, although the resulting precipitate would be more advanced in growth than that usually associated with strain-aging.

The negative creep and the slight serrated effect in the creep curves of the boron heats at 1,600° F and 20,000 psi appear to be additional evidence of strain-induced precipitation. These phenomena have been observed in other nickel-base alloys containing boron in unpublished work in this laboratory.

The presence of strain-aging-type reactions in nickel-base alloys is not totally unexpected. Serrated stress-strain curves have been detected for alloys of 80 percent nickel and 20 percent chromium up to 1,292° F (ref. 20).

Although the preceding evidence indicates that strain-induced carbide precipitate might have lowered creep rate, the proof is not considered positive.

Depletion. - The depletion of γ' definitely required stress. No evidence of its occurrence was observed up to 1,600° F without stress. Furthermore, it was more prevalent in the transverse grain boundaries. The absence of γ' depletion when the alloy was aged at 1,600° F without stress indicates that the reaction was not due to simple depletion of elements forming γ' from the adjoining matrix by the grain-boundary precipitates. It seems probable that the depletion mechanism was strain-induced γ' agglomeration resulting from localized strain concentration at the grain boundaries.

Surface cracking. - The information obtained on surface cracking was not sufficiently extensive to ascertain its role. The indications were that, when boron or zirconium retarded micro-cracking to allow longer creep exposures or more highly stressed creep exposures, fracture was at least in part initiated by surface cracks.

Intragranular γ' stability. - It was at first thought that boron and zirconium might operate through some influence on the size, distribution, or stability of the intragranular γ' reaction. Since reference 10 succeeded in correlating creep-rupture properties with the surface density of γ' particles as measured in electron micrographs, surface density was used to detect possible effects of boron and zirconium on the γ' that would increase rupture life. No significant effect was found. In fact, these elements had so little effect on any aspect of γ' (other than in suppressing agglomeration and depletion of γ' at grain boundaries) that it seems certain that the boron-zirconium effect did not operate through the reaction.

In the absence of any observable effect on the γ', the reason for the higher hardness of heat V + B + Zr is uncertain. It was noted that the hardness values were in the same order as the total titanium plus aluminum in the heats. The slightly higher amounts of titanium and aluminum may account for the higher hardness of heat V + B + Zr.

The distribution of the γ' after creep exposure was a good indicator of the mode and location of creep deformation. Alinement of γ' seemed to indicate that creep deformation had been accommodated by the grains as coarse slip. This alinement had previously been found by reference 21 to indicate the mode of deformation in nickel-base alloys.

Nodular precipitate. - The role of the nodules of mixed carbide and γ' was not clear. No evidence was found to indicate that cracking was initiated by their presence. It is possible that they contributed to the depletion of γ' adjacent to the grain boundaries by acting as a final location for the γ'. This hypothesis is somewhat supported by the accelerating effect of stress on nodular formation at 1,600° F, particularly when γ' depletion occurred.

Relation of Mechanism to Published Information

The accumulation of $M_{23}C_6$ in grain boundaries has striking parallels to sensitization of stainless steels. Reference 22 has identified $Cr_{23}C_6$ as the grain-boundary phase leading to stress-corrosion of 18-8 stainless steels. In addition, reference 16 found the size, shape, and distribution of $Cr_{23}C_6$ in 18-8 stainless steels to be similar to that of $M_{23}C_6$ found in this study.

The agglomeration at grain boundaries during creep of titanium-aluminum-hardened nickel-base alloys has been noted in references 23 and 24. Reference 24 hypothesized that the precipitate was γ' and chromium compounds. Although it was stated that this agglomeration was probably important in determining rupture life, further details of the mechanism were not given.

The γ' and $M_{23}C_6$ network could influence properties in two ways. The $M_{23}C_6$ particles could act as heterogeneous nuclei for micro-cracks, lowering the requirements for micro-cracking. Also, a continuous film in the grain boundaries can lead to stress concentration at the grain boundaries. Strain on the slip planes running up to the grain boundary from one grain cannot pass into the adjoining grain because of blocking by the film (ref. 25). Thus, the opportunity for stress-relief is reduced.

In accordance with the theories of reference 25, depletion of precipitates in layers of matrix adjacent to grain boundaries would promote micro-cracking and fracture by concentrating deformation at these weak grain boundaries. It is possible that this mechanism operates in many high-temperature alloys to give brittle fractures when the creep resistance of the material remains high. Such an explanation was offered in reference 26 for brittle fracture of chromium-nickel-molybdenum steels in long-time service at 500° C. Localized precipitation of Mo_2C left a condition of strong grains and depleted grain boundaries. Further confirmation is obtained from work on the effect of cellular precipitation (refs. 27 and 28), which left depleted regions in the grain boundaries and led to premature and brittle creep-rupture.

The location of micro-cracks at the $M_{23}C_6$-matrix interface was interesting in light of reference 29, which established that ZnO particles were heterogeneous nuclei for micro-cracks in α-brass. As shown by reference 30, particle-matrix bonding is important in nucleation of micro-cracks. In general, the presence of second-phase particles makes nucleation more probable, especially when bonding is poor. Considering these effects, it seems probable that the $M_{23}C_6$ particles acted as nuclei for micro-cracks, possibly because of poor bonding.

The mechanism of nucleation and growth of micro-cracks is not clear. Several authors (refs. 29 to 33) have proposed condensation of vacancies formed during creep by dislocation movements. Others (refs. 25, 34, and 35) emphasized local stress concentrations as the cause. Grain-boundary sliding is usually considered to set up the local stress concentrations at the transverse boundaries to cause loss of cohesion. Reference 25 hypothesizes that the rate of growth of micro-cracks in grain boundaries depends upon the stress pattern at the boundaries. Propagation of

micro-cracking is caused primarily by the normal stress at the grain boundary and the inability of the material to relieve this stress. The over-all rate of growth depends upon the ability of the grains to accommodate the normal stresses by deformation within the grain. From this it can be inferred that micro-cracking increases as the severity of localization of deformation at grain boundaries increases. Therefore, change of the mode of deformation from intragranular slip to grain-boundary creep can be expected to increase grain-boundary micro-cracking by redistribution of stresses. In fact, in α-brass the occurrence of micro-cracking is coincident with the change from coarse slip to grain-boundary sliding (ref. 31). The evidence of increased intragranular slip and decreased micro-cracking in the boron and zirconium heats is in full agreement with these theories. It appears feasible that the elements have changed the mode of deformation by maintaining the grain-boundary strength.

The discrepancies in the literature on the time of micro-crack nucleation are not surprising, considering the effect of trace elements in this study. While several instances have been found of micro-cracking early in second-stage creep (refs. 28 (Nield), 32, and 36), other cases exist where no micro-cracking was found until tertiary creep (refs. 31, 37, and 38). In this study, the case exists where, in one alloy, nucleation of micro-cracks can be delayed from early in second-stage to early in third-stage creep by trace elements.

Regarding the effect of micro-cracks on properties, the Russian theorists (refs. 33, 36, and 39) attribute tertiary creep and rupture to a gradual destruction of the metal by micro-cracking. This implies that micro-cracking raises creep rate and lowers life and ductility. In addition, the normal break in the stress-rupture curve of commercial alloys associated with a change from transgranular to intergranular fracture is an important consideration. This change in fracture mechanism, which is essentially an increase in intergranular micro-cracking, results in lower life and ductility than predicted from higher stress data where micro-cracking was less predominant.

In general, the literature supports the mechanism established. The grain-boundary process would be expected to raise creep rate and lower rupture life and ductility. It follows that retardation of the grain-boundary changes by boron and zirconium would be the mechanism for their beneficial effects on properties.

Causes of Effect of Boron and Zirconium on Grain-Boundary Stability

The experimental evidence established that trace amounts of boron and zirconium retard agglomeration at grain boundaries and thereby retard

the micro-cracking mechanism. Several causes of this retardation of agglomeration might be proposed.

It can be hypothesized that boron and zirconium stabilize carbon directly in a less deleterious form than intergranular $M_{23}C_6$ in the same manner that titanium stabilizes carbon as TiC in 18-8 stainless steels. One would expect to find evidence of boron-carbon or zirconium-carbon compounds in this case. Since none were detected, support for this theory is lacking.

A similar possibility would be that the elements are promoting stabilization of carbon indirectly by promoting the nucleation and growth of one carbide at the expense of another. This might result from solid solution of boron or zirconium in the complex carbides of the M_6C or $M_{23}C_6$ type. Indeed, the detection of intragranular carbides, apparently the M_6C type, when boron was present is compatible with this hypothesis. However, lack of promotion of additional carbides by zirconium additions does not support this hypothesis.

An alternative reason might be found in equilibrium segregation. The relations of grain boundaries to impurity distribution are reviewed in reference 40. When elements of odd atomic size exist in alloys, they are subject to inhomogeneous distribution. Because they do not fit well in the crystal lattice where high regularity exists, the odd-sized atoms segregate to regions of lower regularity where larger vacancies exist. Grain boundaries are a principal region of concentration because of their inherent irregularity. Experimental confirmation for this was obtained in reference 41, which showed that polonium segregates to grain boundaries in lead-bismuth alloys. The segregating tendencies of two competing odd-sized elements can be related to their degree of misfit in that the most odd-sized atoms will seek out the grain boundary more rapidly. Thus, small amounts of one very odd-sized element can be utilized to heal the grain boundary, thereby retarding the segregation of a less odd-sized element by decreasing the available holes in the grain boundary. The possibility exists that boron and zirconium are retarding carbon segregation by this mechanism.

Study of the atomic diameters of carbon, boron, and zirconium might reveal the feasibility of this theory. Reference 42 shows that the effective diameter of carbon in γ-iron is 1.36 angstroms, while it is postulated that boron has an effective diameter equivalent to or greater than 1.85 to 1.90 angstroms. Goldschmidt's effective diameter (for coordination number of 12) for zirconium is 3.20 angstroms. The available lattice spaces in the alloy of 55 percent nickel, 20 percent chromium, 15 percent cobalt, 4 percent molybdenum, 3 percent titanium, and 3 percent aluminum can be calculated from the lattice parameter of 3.58 angstroms established in unpublished work at this laboratory. The vacant interstitial space in

solid solution is 1.05 angstroms in diameter. Using the data on atomic diameters, the carbon atom is 30 percent larger, boron is 78 percent larger, and zirconium is 200 percent larger than the available space. In the case of substitutional solution, the boron atom is approximately 26 percent smaller and zirconium 26 percent larger than the substitutional space of 2.53-angstrom diameter. Therefore, it appears that carbon fits moderately well interstitially but that boron and zirconium fit poorly both as interstitials and in substitution. Then it seems feasible that boron and zirconium are segregating preferentially to grain boundaries, healing them and retarding carbon segregation.

Other aspects of the data lend support to the theory of equilibrium segregation. Decreased tendency for γ' agglomeration at the grain boundaries of the boron and zirconium heats could result from the boron and zirconium healing of the grain boundaries. The promotion of intragranular carbide by boron might be the indirect result of this. The decreased segregation would leave a higher carbon content within the grains, making precipitation of intragranular carbides more probable.

Additional support for the theory of equilibrium segregation is in the literature. Reference 43 proposed that boron additions benefit iron-base alloys by this mechanism. Reference 44 emphasized that marked improvement of properties by trace-element additions usually occurs with elements with characteristics that would lead to segregation to grain boundaries.

Role of Carbon

The apparent harmful effect of $M_{23}C_6$ in the grain boundaries of the alloy and the possible helpful effect of the intragranular carbide promoted by boron make the role of carbon in nickel-base alloys of great interest.

One might conclude from the results that the relatively carbon-free alloy would be free of the grain-boundary carbide agglomeration and therefore have properties equivalent to heat V + B + Zr. However, this is not the case. Unpublished work at this laboratory shows that both rupture life and ductility increase as carbon is increased from less than 0.01 to 0.04 percent in the boron- and zirconium-free alloy. Therefore, it seems that carbon can also have a beneficial role in the alloy. The reason for this effect is not at all clear at this time, but it could be one of several mechanisms including improved degassing, solid-solution strengthening, or prevention of other embrittling grain-boundary reactions.

Generality of Results

The beneficial effects of boron and zirconium in nickel-base titanium-aluminum refractory alloys are commonly known. Properties of such alloys in the absence of these elements will generally be inferior to their properties when the proper amounts are present. The particular alloy used to study the boron-zirconium mechanism is certainly not unusual in this respect. The results presented do in fact increase the confidence that can be placed in the alloy studied through clarification of the mechanism involved.

It is confidently expected that the basic mechanism established for the influence of trace amounts of boron and zirconium will be generally applicable. However, there will be variants in individual alloys and within a specific alloy depending on prior history, heat treatment, and testing conditions. With this in mind, the limitations of the present results should be clearly recognized. Only one alloy with one heat treatment was studied. The test conditions were limited to 1,600° F on material made in a small vacuum furnace and hot-worked under idealized laboratory conditions.

In the type of alloy considered, it is expected that boron and zirconium will generally operate through two phenomena: They suppress the formation of noncoherent phases in the grain boundaries, and they also retard the rate at which γ' is depleted from the matrix adjacent to the grain boundaries. Both of these factors have been shown to cause weakening of the grain boundaries which subsequently leads to microcracking. Both the details of the mechanism and the effectiveness can be expected to vary, depending on the major alloying elements in specific alloys and the variations of other elements in trace amounts. Because such factors as grain size, carbide composition and distribution, and cold work are sensitive to prior history, the effectiveness of the boron and zirconium can be expected to vary with the basic microstrueture of the alloy. It should be recognized that the boron and zirconium must be present in an effective form. For instance, they must be added under conditions where their effectiveness is not nullified by reaction with oxygen or nitrogen.

The mechanism of creep can be expected to vary with test temperatures and stress. Conditions that favor creep within the grains (temperatures on the low side of the creep range and high stresses) apparently should reduce the effectiveness of boron and zirconium under the mechanism observed. Variations in the conditions of formation of γ' or in the amounts through variation in titanium and aluminum should also be involved. It is becoming evident through research efforts of others that the type of carbide formed can depend on temperature and time. Again, this should alter the effectiveness of the boron-zirconium reaction.

Reference 1 showed that there can be sharp optimums in the properties depending on the amounts of boron plus zirconium. This aspect of

the mechanism has not yet been established, although it is expected that it will arise from some modification of the observed mechanism. This reference also showed that boron and zirconium up to limiting amounts were very effective in reducing cracking during hot-working. This demonstrates that they are effective at temperatures much higher than 1,600° F. It is not certain that the same mechanism observed at 1,600° F is involved.

Boron, at least, is effective in raising creep-rupture properties of types of alloys other than the nickel-base titanium-aluminum alloys. The results of this investigation suggest that it may operate in these cases through modification of carbide reactions. The further possibility also exists that boron, by itself or through modification of carbon-nitrogen reactions, introduces strain-aging-type reactions.

SUMMARY OF RESULTS

Investigation of the effects of adding trace amounts of boron and zirconium to a complex titanium-aluminum-hardened nickel-base alloy gave the following results:

1. The creep-rupture properties of the alloy were improved by retarding structural changes at the grain boundaries. In the absence of these elements, $M_{23}C_6$ and γ' agglomerated rapidly in the grain boundaries. Subsequently, the matrix material adjacent to the grain boundaries transverse to the applied stress became depleted of γ' precipitates. Micro-cracks then developed at the $M_{23}C_6$-depleted-matrix interfaces, grew, and combined to initiate brittle and premature fracture.

2. Zirconium, boron, and boron plus zirconium in the proper amounts retarded these changes, effectiveness increasing in the order listed, to allow longer life to higher deformations before fracture occurred. While micro-cracking was detected early in second-stage creep at relatively short time periods in the absence of boron and zirconium, proper amounts of boron and zirconium delayed micro-cracking until after third-stage creep started after long creep exposure.

3. Creep-rupture properties at 1,600° F of the material correlated with the stability of the grain boundaries. The property effects were not found to result from a change in the size, amount, and distribution of the general intragranular γ'.

4. Some possible causes of the stabilizing influence of boron and zirconium on the grain boundaries were discussed. Of these, retardation of agglomeration by preferential segregation of boron and zirconium to grain boundaries fits the data best.

University of Michigan,
Ann Arbor, Mich., October 11, 1957.

REFERENCES

1. Decker, R. F., Rowe, John P., and Freeman, J. W.: Influence of Crucible Materials on High-Temperature Properties of Vacuum-Melted Nickel-Chromium-Cobalt Alloy. NACA TN 4049, 1957.

2. Koffler, R. W., Pennington, W. J., and Richmond, F. M.: The Effect of Small Amounts of Boron and Zirconium on the High Temperature Properties of Vacuum-Melted Super Alloys. Rep. 48, Res. and Dev. Dept., Universal-Cyclops Steel Corp., June 11, 1956.

3. Jones, W. E.: Vacuum Induction Melting-Process Considerations. Metal Prog., vol. 72, no. 4, Oct. 1957, pp. 133-138; 220-222.

4. Nordheim, R., and Grant, N. J.: Aging Characteristics of Nickel-Chromium Alloys Hardened with Titanium and Aluminum. Jour. Metals, vol. 6, no. 2, sec. 2, Feb. 1954, pp. 211-218.

5. Taylor, A.: Constitution of Nickel-Rich Quaternary Alloys of the Ni-Cr-Ti-Al System. Jour. Metals, vol. 9, no. 1, sec. 2, Jan. 1957, pp. 71-75.

6. Betteridge, W., et Franklin, A. W.: Les Progrès des alliages à base de nickel-chrome en service à haute température. Revue de mètallurgie, t. 53, no. 4, Apr. 1956, pp. 271-284.

7. Frey, D. N., Freeman, J. W., and White, A. E.: Fundamental Aging Effects Influencing High-Temperature Properties of Solution-Treated Inconel X. NACA TN 2385, 1951.

8. Brockway, L. O., and Bigelow, W. C.: The Investigation of the Minor Phases of Heat-Resistant Alloys by Electron Diffraction and Electron Microscopy. TR 54-589, WADC, May 1955. (Contract AF-33(616)-23.)

9. Betteridge, W., and Smith, R. A.: Effect of Heat Treatment and Structure Upon Creep Properties of Nimonic Alloys Between 750° and 950° C. Symposium on Metallic Materials for Service at Temperatures Above 1600° F, Spec. Tech. Pub. 174, ASTM, 1956, p. 29.

10. Baillie, Y.: Quelques résultats de l'étude au microscope électronique des alliages Ni-Cr-Al-Ti employés dans les turbines aéronautiques. Revue Univ. des Mines, t. 12, no. 10, ser. 9, Oct. 1956, pp. 507-512.

11. Beattie, H. J., and VerSnyder, F. L.: The Influence of Molybdenum on the Phase Relationships of a High Temperature Alloy. Trans. ASM, vol. 49, 1957, pp. 883-895; discussion, pp. 895-904.

12. Wilde, Robert F., and Grant, Nicholas J.: Aging in Complex Commercial Ni-Cr Alloys Hardened with Titanium and Aluminum. Jour. Metals, vol. 9, no. 7, sec. 2, July 1957, pp. 865-872.

13. Betteridge, W., and Franklin, A. W.: The Effect of Heat-Treatment and Structure on the Creep and Stress-Rupture Properties of Nimonic 80A. Jour. Inst. Metals, vol. 85, pt. II, 1957, pp. 473-479.

14. Bigelow, W. C., Amy, J. A., and Brockway, L. O.: Electron Microscopic Identification of the γ' Phase of Nickel-Base Alloys. Proc. ASTM, vol. 56, 1956, pp. 945-953.

15. Fisher, R. M.: Electron Microstructure of Steels by "Extraction Replica" Technique. Symposium on Techniques for Electron Metallography, Spec. Tech. Pub. 155, ASTM, 1953, pp. 49-63; discussion pp. 63-64.

16. Plateau, J., Henry, G., et Crussard, C.: Quelques nouvelles applications de la microfractographie. Revue de Mètallurgie, t. 54, no. 3, Mar. 1957, pp. 200-216.

17. Bradley, D. E.: Evaporated Carbon Films for Use in Electron Microscopy. British Jour. Appl. Phys., vol. 5, Feb. 1954, pp. 65-66.

18. Fullam, Ernest F.: Replica Washing Methods. Symposium on Techniques for Electron Metallography, Spec. Tech. Pub. 155, ASTM, 1953, pp. 101-106; discussion, pp. 107-108.

19. Cottrell, A. H.: Creep and Aging Effects in Solid Solutions. Symposium on Creep and Fracture of Metals at High Temperatures, (May 31-June 2, 1954), Nat. Phys. Lab. (London), 1956, pp. 141-152; discussion, pp. 153-155.

20. Waché, Xavier: Allongement discontinu des austénites soumises à l'essai de traction ordinaire à hautes températures. Comptes Rendus, t. 240, May 1955, pp. 1892-1896.

21. Bueckle, C., et Poulignier, J.: Étude mètallographique de l'écrouissage dans les alliages du type nickel-chrome, 80/20 tenaces à chord. Revue de métallurgie, t. 53, no. 3, Mar. 1956, pp. 179-188.

22. Bungardt, Karl, und Lennartz, Gustav: Ausscheidungsvorgänge in einem mit Titan stabilisierten austenitischen Chrom-Nickel-Stahl und ihre Beziehung zur interkristallinen Korrosion. Arch. f. das Eisenhuttenwesen, Jahrg. 27, Heft 2, Feb. 1956, pp. 127-133.

23. Baillie, Y., et Poulignier, J.: Étude de la precipitation submicroscopique dans les alliages refractaires nickel-chrome. Revue de métallurgie, t. 51, no. 3, Mar. 1954, pp. 179-190; discussion, pp. 190-191.

24. Mathieu, M.: Contribution à la connaissance des alliages Ni-Cr 80/20 modifiés résistant a chaud. La Récherche Aéro., no. 51, May-June 1956, pp. 43-51.

25. Chang, H. C., and Grant, Nicholas J.: Mechanism of Intercrystalline Fracture. Jour. Metals, vol. 8, no. 5, sec. 2, May 1956, pp. 544-551.

26. Wever, Franz, und Schrader, Angelica: Elektronenmikroskopische Untersuchung der Gefügeveränderungen eines Chrom-Nickel-Molybdän-Stahles unter langzeitiger Zugbeanspruchung bei 500°. Arch. f. das Eisenhuttenwesen, Jahrg. 26, Heft 8, Aug. 1955, pp. 475-481.

27. Roberts, C. S.: Interaction of Precipitation and Creep in Mg-Al Alloys. Jour. Metals, vol. 8, no. 2, sec. 2, Feb. 1956, pp. 146-148.

28. Betteridge, W.: Tertiary Creep of Nimonic 80A. Symposium on Creep and Fracture of Metals at High Temperatures, (May 31-June 2, 1954), Nat. Phys. Lab. (London), 1956, pp. 299-307. (Discussion by A. H. Sully, p. 308; discussion by B. J. Nield, pp. 308-311.)

29. Resnick, R., and Seigle, L.: Nucleation of Voids in Metals During Diffusion and Creep. Jour. Metals, vol. 9, no. 1, sec. 2, Jan. 1957, pp. 87-93.

30. Machlin, E. S.: Creep-Rupture by Vacancy Condensation. Jour. Metals, vol. 8, no. 2, sec. 2, Feb. 1956, pp. 106-111.

31. Greenwood, J. N., Miller, D. R., and Suiter, J. W.: Intergranular Cavitation in Stressed Metals. Acta Metallurgica, vol. 2, no. 2, Mar. 1954, pp. 250-258.

32. Crussard, C., and Friedel, J.: Theory of Accelerated Creep and Rupture. Symposium on Creep and Fracture of Metals at High Temperatures, (May 31-June 2, 1954), Nat. Phys. Lab. (London), 1956, pp. 243-262.

33. Guy, A. G.: Russian Theory for Creep Fracture. Metal Prog., vol. 69, no. 3, Mar. 1956, pp. 158-160.

34. McLean, D.: A Note on the Metallography of Cracking During Creep. Jour. Inst. Metals, vol. 85, pt. II, July 1957, pp. 468-471; discussion, pp. 471-472.

35. Nield, B. J., and Quarrell, A. G.: Intercrystalline Cracking in Creep of Some Aluminum Alloys. Jour. Inst. Metals, vol. 85, pt. II, July 1957, pp. 480-485; discussion, pp. 485-488.

36. Kishkin, S. T.: Mechanism of Weakening and Fracture of Crystalline Bodies as a Function of Time at High Temperature. Akad. Nauk SSSR Doklady, vol. 95, 1954, pp. 789-791. (Russian)

37. McAdam, D. J., Jr., Giel, G. W., and Woodard, D. H.: Influence of Strain Rate and Temperature on the Mechanical Properties of Monel Metal and Copper. Proc. ASTM, vol. 46, 1946, pp. 902-950.

38. Grant, N. J.: Grain Boundary Participation in Creep Deformation and Fracture. Symposium on Creep and Fracture of Metals at High Temperatures, (May 31-June 2, 1954), Nat. Phys. Lab. (London), 1956, pp. 317-330. Discussion by H. W. Kirby, p. 331.

39. Dekhtiar, I. I., and Osipov, K. A.: Fracture of Metals at High Temperatures. Akad. Nauk SSSR Doklady, vol. 104, no. 2, 1955, pp. 229-232. (Russian)

40. Cahn, R. W.: Grain Boundaries, Substructures and Impurities. ASM Seminar on Impurities and Imperfections, Thirty-Sixth Nat. Metal Congress and Exposition (Chicago), Oct. 30-Nov. 5, 1955, pp. 41-83.

41. Thomas, W. R., and Chalmers, B.: The Segregation of Impurities to Grain Boundaries. Acta Metallurgica, vol. 3, no. 1, Jan. 1955, pp. 17-21.

42. Speiser, Rudolph, Spretnak, J. W., and Taylor, W. J.: Effective Diameter of Solute Atoms in Interstitial Solid Solutions. Trans. ASM, vol. 46, 1954, pp. 1168-1175.

43. Brown, J. T., and Bulina, J. W.: W-545 - A New Higher Temperature Turbine Disc Alloy. Paper presented at Regional High-Temperature Materials Conf., Cleveland Sec. of AIME, Apr. 16, 1957. (To be pub. by AIME.)

44. Strauss, Jerome: Micrometallurgy: The Metallurgy of Minute Additions. Proc. ASTM, vol. 53, 1953, pp. 577-595.

TABLE I. - CHEMICAL ANALYSES OF EXPERIMENTAL HEATS

Heat	Weight-percent as-rolled														
	B	Zr	Cr	Co	Mo	Ti	Al	Si	Mn	C	S	P	Mg	Fe	Cu
V	0.0002	<0.01	19.7	15.0	3.90	3.08	3.35	0.17	0.13	0.08	0.007	0.006	<0.01	<0.30	<0.10
V + Zr	0.0004	0.19	18.8	15.1	4.15	3.14	3.14	0.10	<0.10	0.08	0.008	0.003	-----	<0.30	-----
V + B	0.0089 [a].0090 [b].0079	<0.01	20.9	14.8	4.20	3.15	3.25	0.20	<0.10	0.10	-----	0.004	<0.01	<0.30	<0.10
V + B + Zr	0.0088	0.01	20.8	14.8	4.20	3.20	3.30	0.19	0.11	0.09	-----	0.007	<0.01	<0.30	<0.10

[a]Analysis on cross section of 0.250-in.-diam. rupture specimen after 428 hr at 1,600° F.
[b]Analysis on 0.010-in. surface layer of sample described in footnote a.

TABLE II. - CREEP-RUPTURE DATA AT 1,600° F

[Initial condition: 2 hr at 2,150° F, air-cooled, + 4-hr preheat at 1,600° F before loading.]

Heat	Stress, psi	Minimum second-stage creep rate, %/hr	Rupture			Interruption	
			Time, hr	Elongation, %	Reduction of area, %	Time, hr	Total deformation, %
V	25,000	0.0160	45	2	1	---	-----
		.0060	52	2	1	---	-----
	20,000	0.0070	158	3	2	---	-----
		.0040	---	--	--	165	1.23
		.0058	---	--	--	117	1.00
		.0046	---	--	--	85	.76
		.0052	---	--	--	85	.76
		.0084	---	--	--	47	.55
		.0058	---	--	--	23	.29
V + Zr	25,000	0.0036	147	5	5	---	-----
		.0095	134	6	8	---	-----
	22,500	0.0032	208	5	4	---	-----
		.0036	---	--	--	172	1.25
	20,000	0.0027	---	--	--	165	0.63
V + B	28,000	0.0025	298	10	14	---	-----
		.0040	---	--	--	214	3.45
		------	---	--	--	188	1.21
		.0046	---	--	--	68	.56
	25,000	0.0018	429	10	11	---	-----
		------	394	7	8	---	-----
	20,000	Negative	---	--	--	165	0.15
V + B + Zr	30,000	0.0021	266	8	9	---	-----
		------	---	--	--	214	1.18
	25,000	0.0004	666	17	16	---	-----
		.0003	627	12	13	---	-----
	20,000	Negative	---	--	--	165	0.04

TABLE III. - PROPERTIES OF SPECIMENS STRESS-AGED AT 1,600° F

Condition	Heat V				Heat V + Zr				Heat V + B				Heat V + B + Zr			
	Nodules (a)	γ' density (b)	Depleted grain boundaries (c)	Micro-cracks (d)	Nodules (a)	γ' density (b)	Depleted grain boundaries (c)	Micro-cracks (d)	Nodules (a)	γ' density (b)	Depleted grain boundaries (c)	Micro-cracks (d)	Nodules (a)	γ' density (b)	Depleted grain boundaries (c)	Micro-cracks (d)
Equal-strain-rate study																
0.5% Creep deformation	259	---	49	5	---	---	---	---	---	---	---	---	--	---	---	---
0.6% Creep deformation	301	---	76	17	---	---	---	---	5	---	2	2	--	---	---	---
0.8% Creep deformation	332	---	184	34	---	---	---	---	---	---	---	---	--	---	---	---
	288	---	173	31	---	---	---	---	---	---	---	---	--	---	---	---
1.0% Creep deformation	334	---	151	116	---	---	---	---	---	---	---	---	--	---	---	---
1.2% Creep deformation	418	134	264	314	176	137	127	78	63	187	60	30	20	117	23	2
3.5% Creep deformation	---	---	---	---	---	---	---	---	79	---	165	77	--	---	---	---
Ruptured	532	---	764	968	228	---	568	532	176	---	676	243	86	---	538	198
Equal-stress study																
165 Hr at 20,000 psi	418	154	264	314	129	151	72	9	25	158	16	None detected	0	125	None detected	None detected
Ruptured at 25,000 psi	225	256	192	574	254	109	916	145	145	67	442	188	86	51	561	402
	218	---	211	378	---	---	---	---	---	---	---	---	90	---	550	330

[a]Mixed carbide and γ' nodule greater than 5 microns diam.; number in 0.008 sq in.
[b]γ' particles per sq in. at 12,000 diam.
[c]Grain boundaries where depletion was detected at 1,000 diam.; number in 0.008 sq in.
[d]Micro-cracks detected at 1,000 diam.; number in 0.008 sq in.

TABLE IV. - PROPERTIES OF SPECIMENS AGED AT 1,600° F WITHOUT STRESS

Aging time, hr	Heat V			Heat V + Zr			Heat V + B			Heat V + B + Zr		
	DPH	Nodules (a)	γ' density (b)	DPH	Nodules (a)	γ' density (b)	DPH	Nodules (a)	γ' density (b)	DPH	Nodules (a)	γ' density (b)
0.5	359	---	---	354	---	---	357	---	---	373	--	---
1	364	---	---	362	---	---	362	---	---	380	--	---
4	359	---	---	353	---	---	357	---	---	368	--	---
10	355	46	588	348	32	544	348	16	788	362	0	584
100	345	180	134	348	57	147	346	33	188	356	19	137
188	338	---	107	342	---	118	340	---	101	353	--	103
500	335	300	85	344	139	87	339	149	88	344	25	84

[a]Nodules greater than 5 microns diam.; number in 0.008 sq in.
[b]γ' particles per sq in. at 12,000 diam.

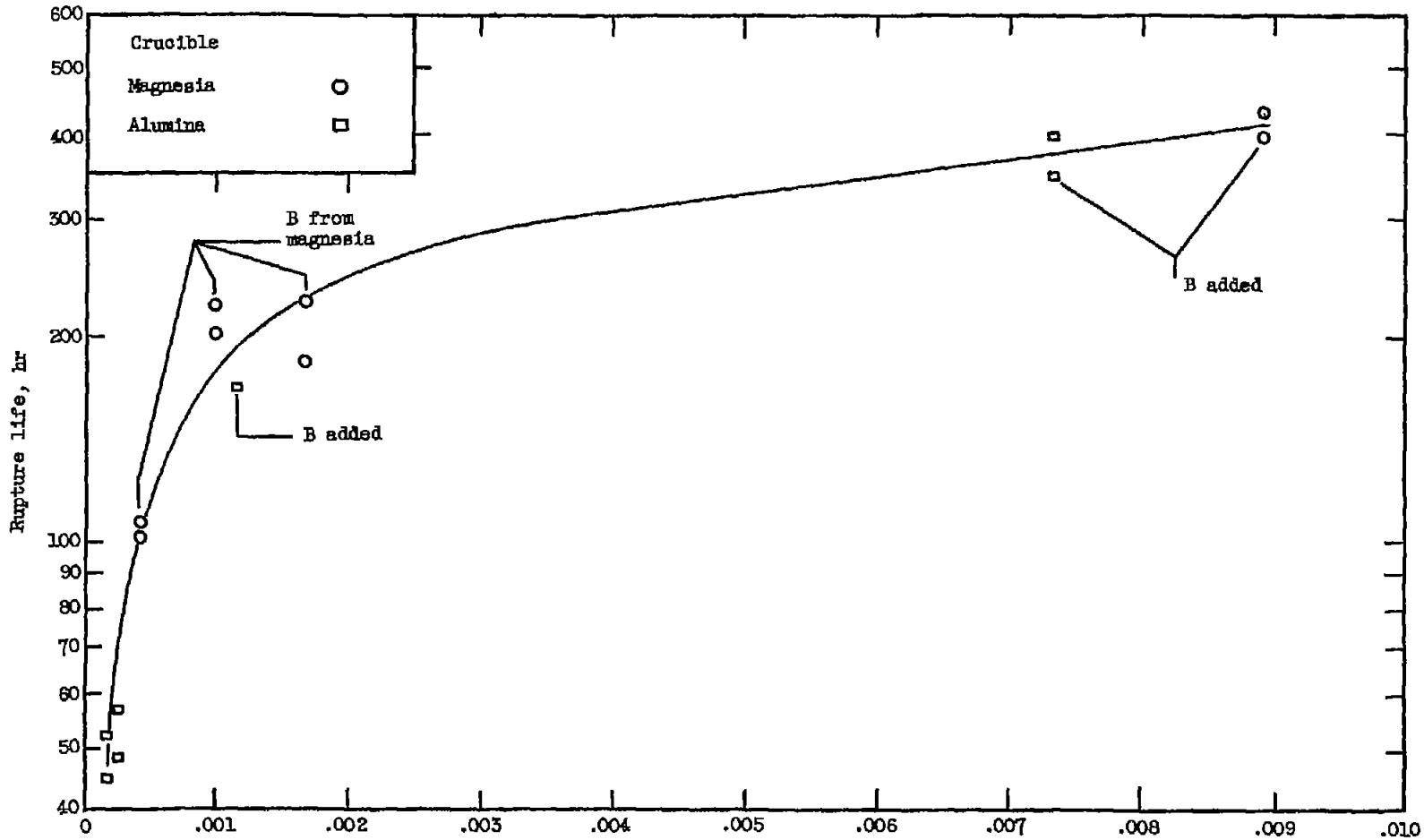

(a) Rupture life.

Figure 1. - Effect of boron content on rupture life and ductility at 1,600° F and 25,000 psi of experimental heats of alloy composed of 55 percent nickel, 20 percent chromium, 15 percent cobalt, 4 percent molybdenum, 3 percent titanium, and 3 percent aluminum (with less than 0.01% Zr). Heat treatment prior to testing: 2 hours at 2,150° F, air-cooled, plus 4-hour preheat at 1,600° F (ref. 1).

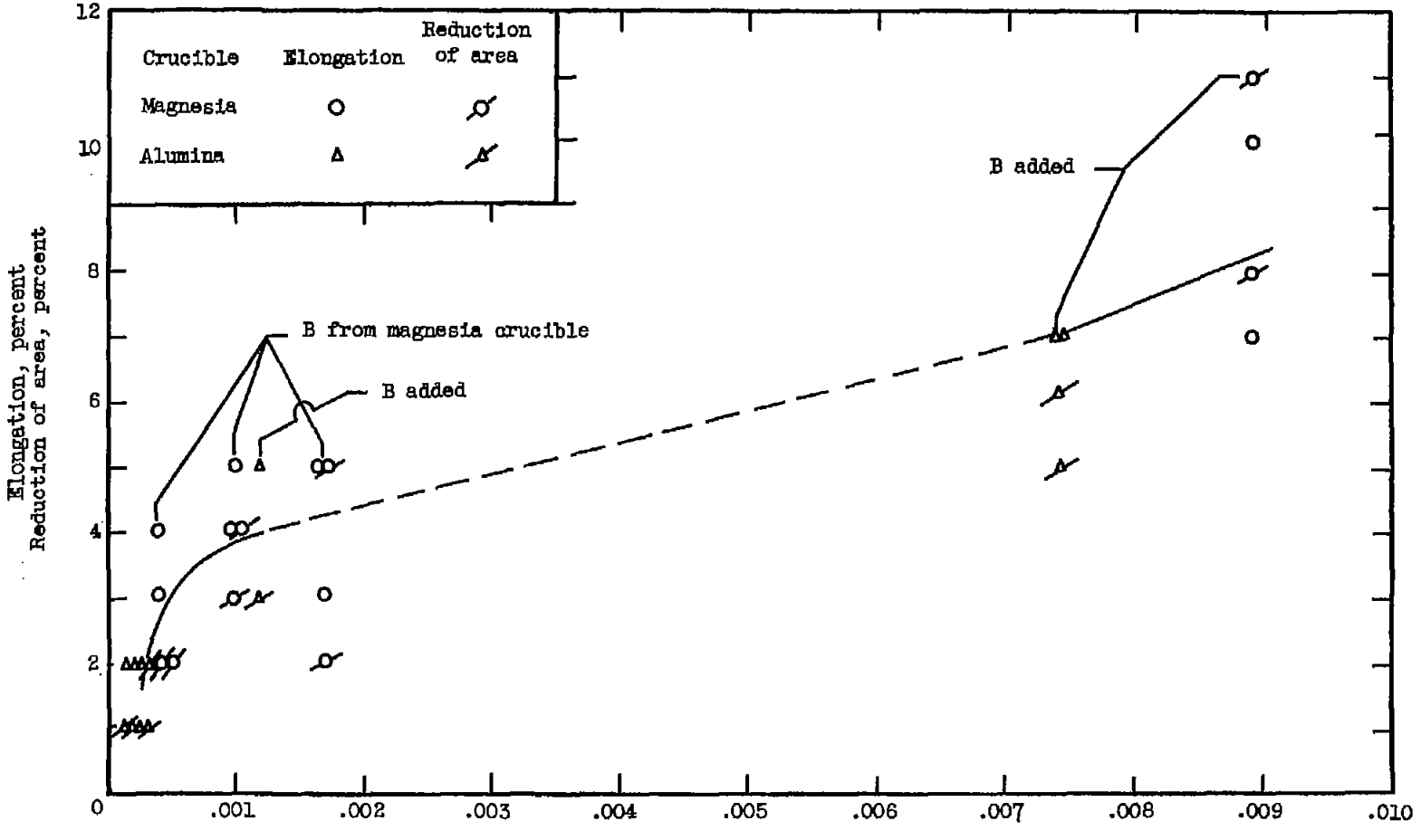

(b) Ductility.

Figure 1. - Concluded.

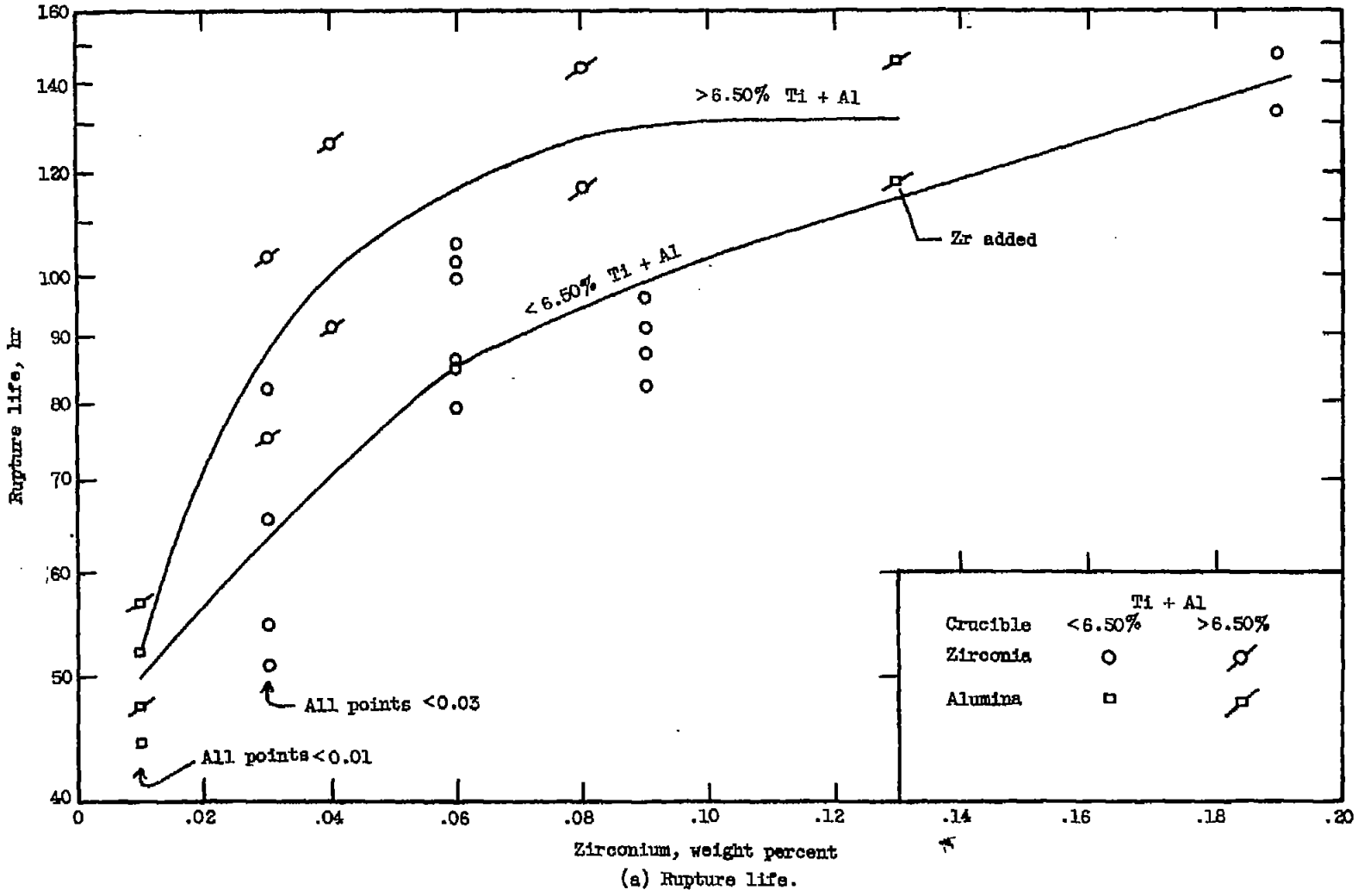

(a) Rupture life.

Figure 2. - Effect of zirconium content on rupture life and ductility at 1,600° F and 25,000 psi of experimental heats of alloy composed of 55 percent nickel, 20 percent chromium, 15 percent cobalt, 4 percent molybdenum, 3 percent titanium, and 3 percent aluminum (with less than 0.0005% B). Heat treatment prior to testing: 2 hours at 2,150° F, air-cooled, plus 4-hour preheat at 1,600° F (ref. 1).

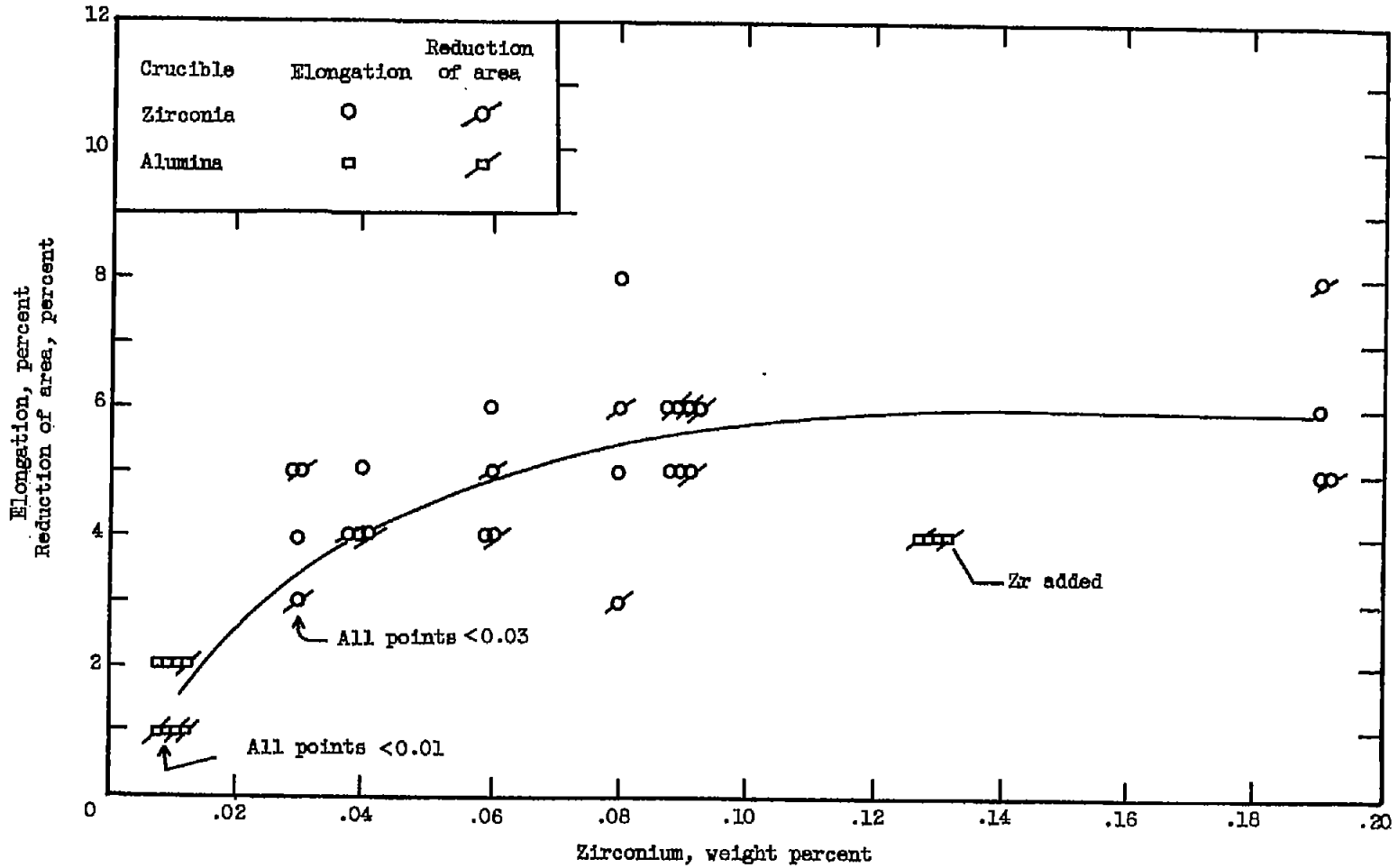

(b) Ductility (with 0.04 to 0.09% C).

Figure 2. - Concluded.

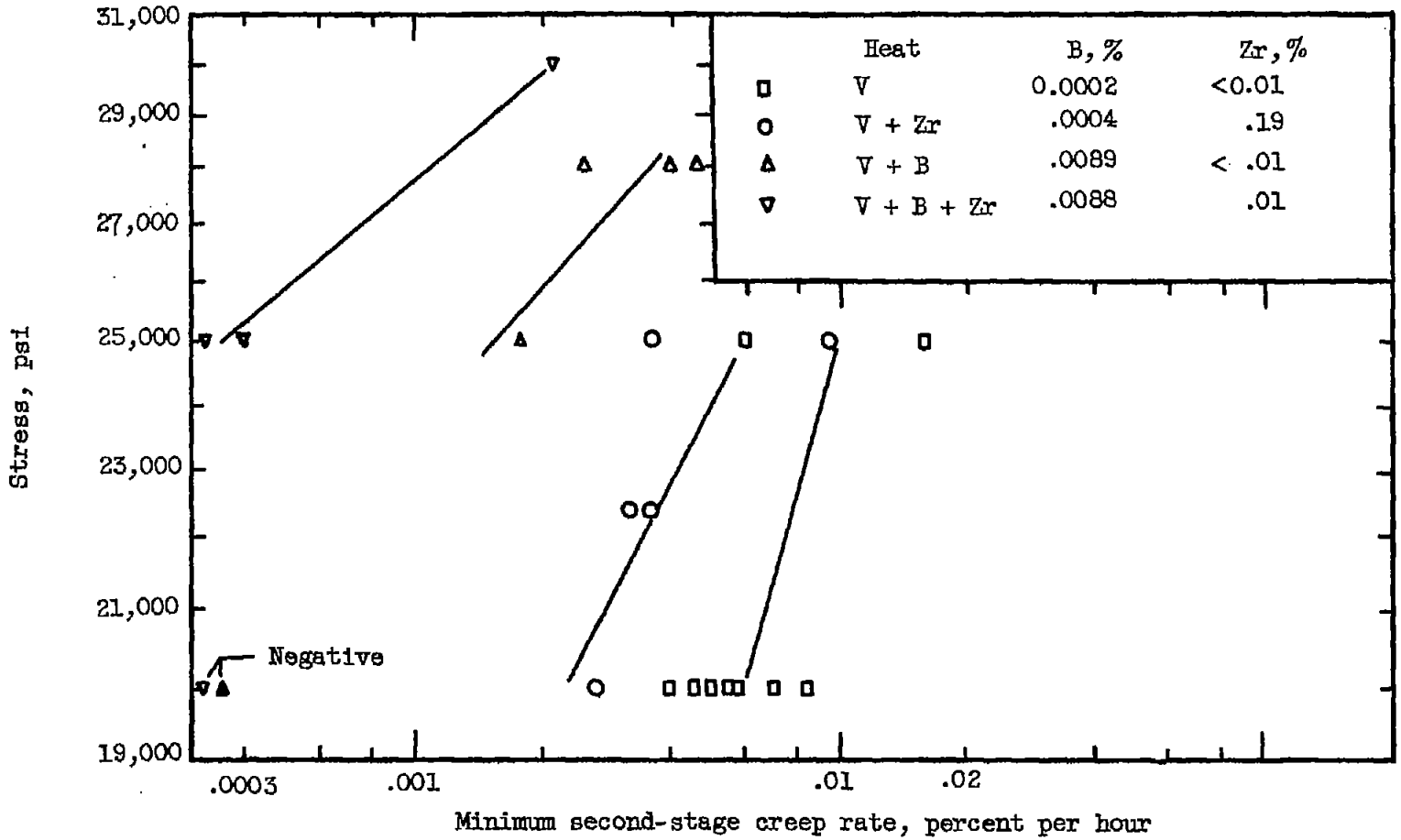

Figure 3. - Influence of stress on minimum second-stage creep rate at 1,600° for experimental heats.

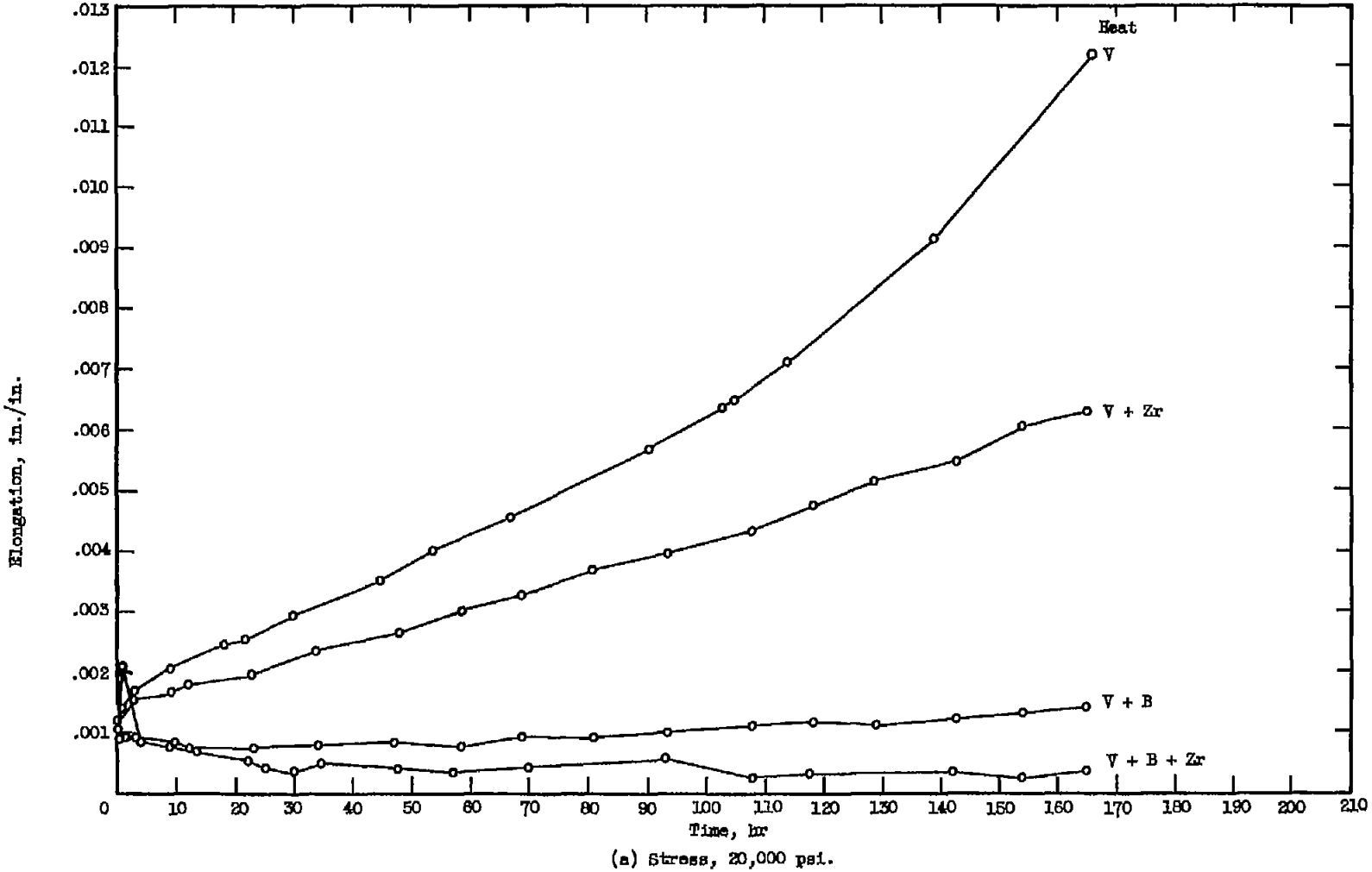

(a) Stress, 20,000 psi.

Figure 4. - Comparative creep curves at 1,600° F for experimental heats.

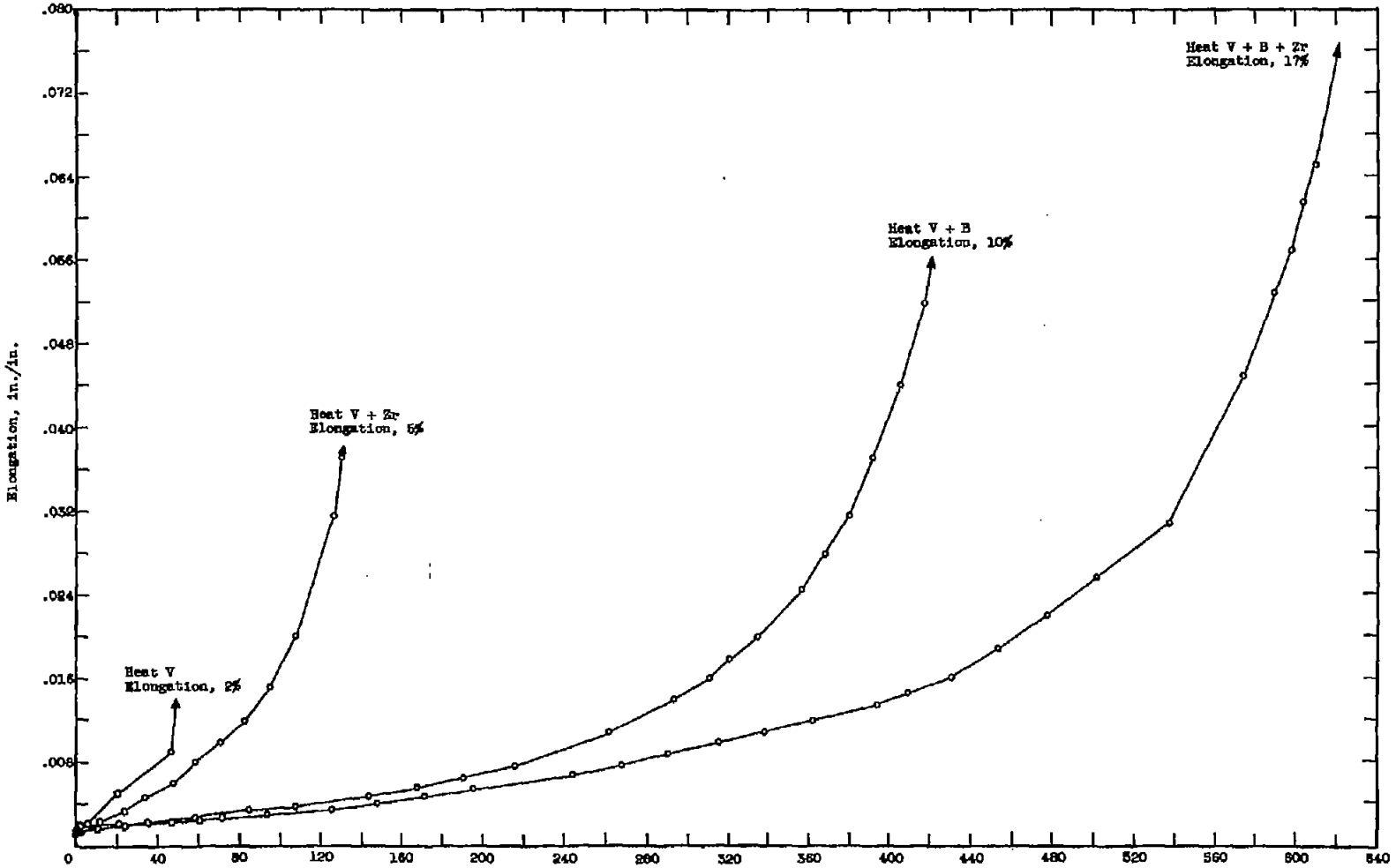

(b) Stress, 25,000 psi.

Figure 4. - Concluded.

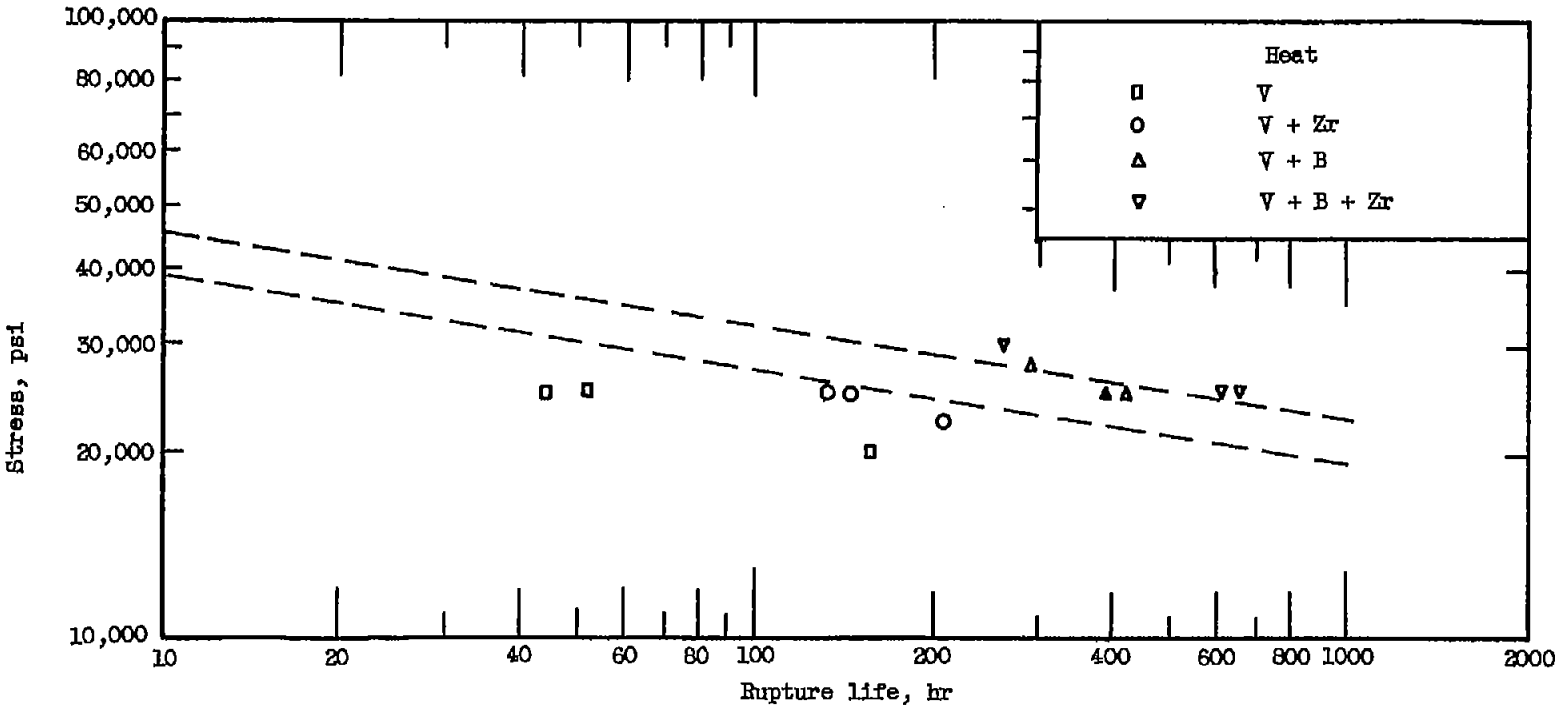

Figure 5. - Effect of stress on rupture life of experimental alloys at 1,600° F. Heat treatment prior to testing: 2 hours at 2,150° F, air-cooled, plus 4-hour preheat at 1,600° F. (Data plotted on dashed rupture band for two heats of commercial 55% Ni, 20% Cr, 15% Co, 4% Mo, 3% Ti, 3% Al alloy (Udimet 500) as reported by Utica Drop Forge and Tool Division of Kelsey-Hayes Co. Heat treatment for commercial alloy: 2 hr at 2,150° F, air-cooled; plus 4 hr at 1,975° F, air-cooled; plus 24 hr at 1,550° F, air-cooled; plus 16 hr at 1,400° F, air-cooled.)

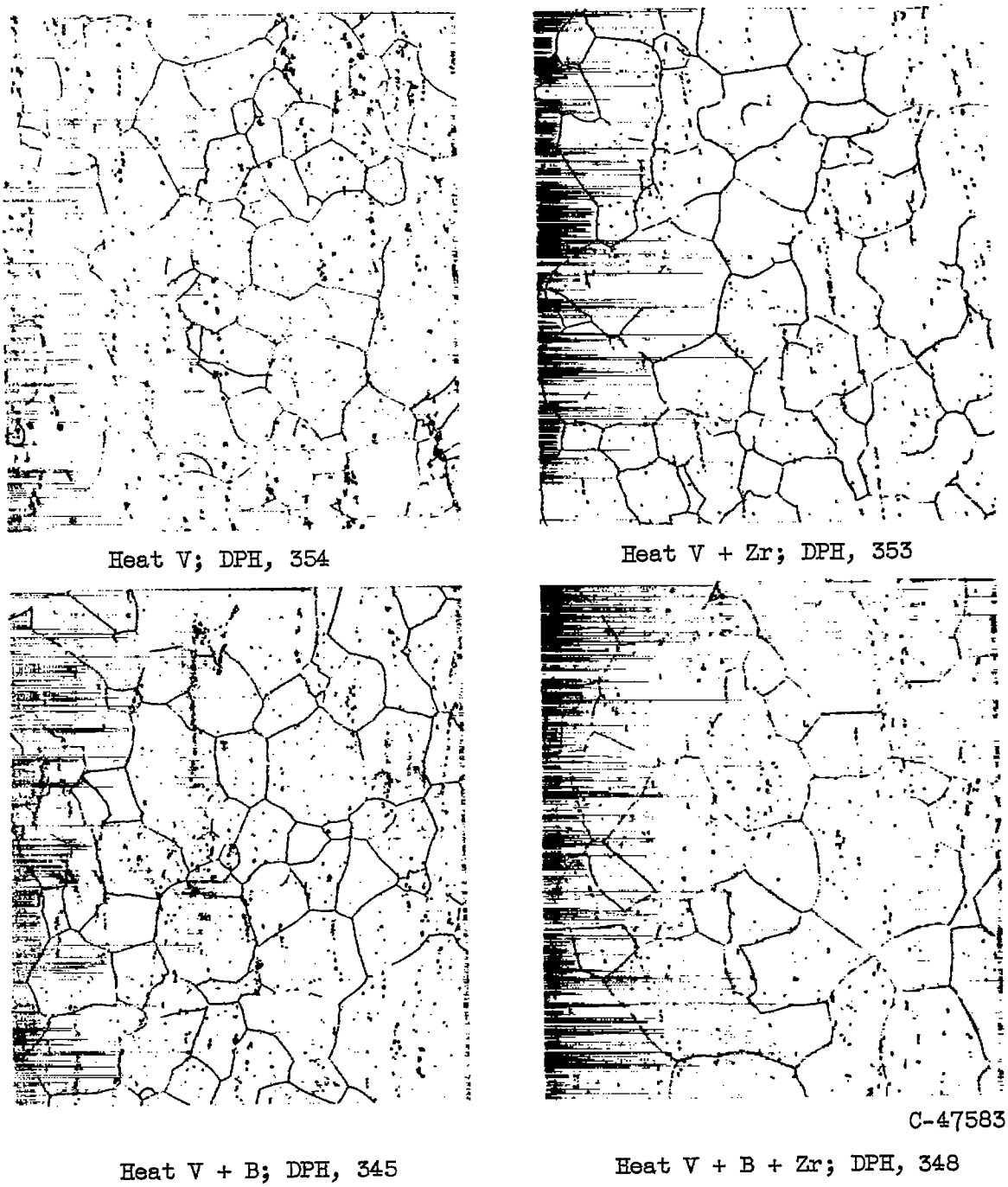

Heat V; DPH, 354

Heat V + Zr; DPH, 353

Heat V + B; DPH, 345

Heat V + B + Zr; DPH, 348

C-47583

(a) Magnification, X100.

Figure 6. - Initial condition of experimental heats as treated 2 hours at 2,150° F and air-cooled.

4933

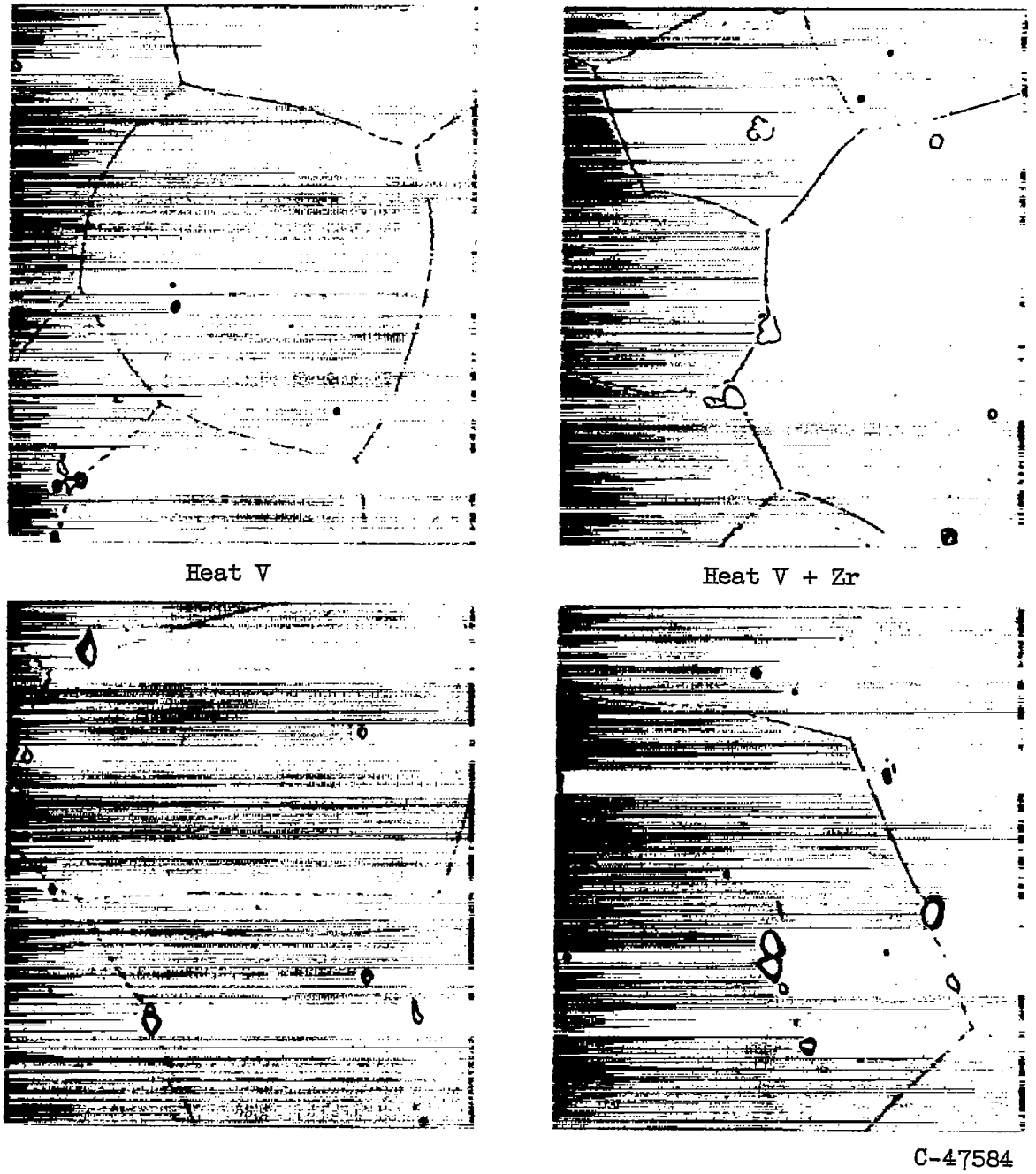

(b) Magnification, X1,000.

Figure 6. - Continued.

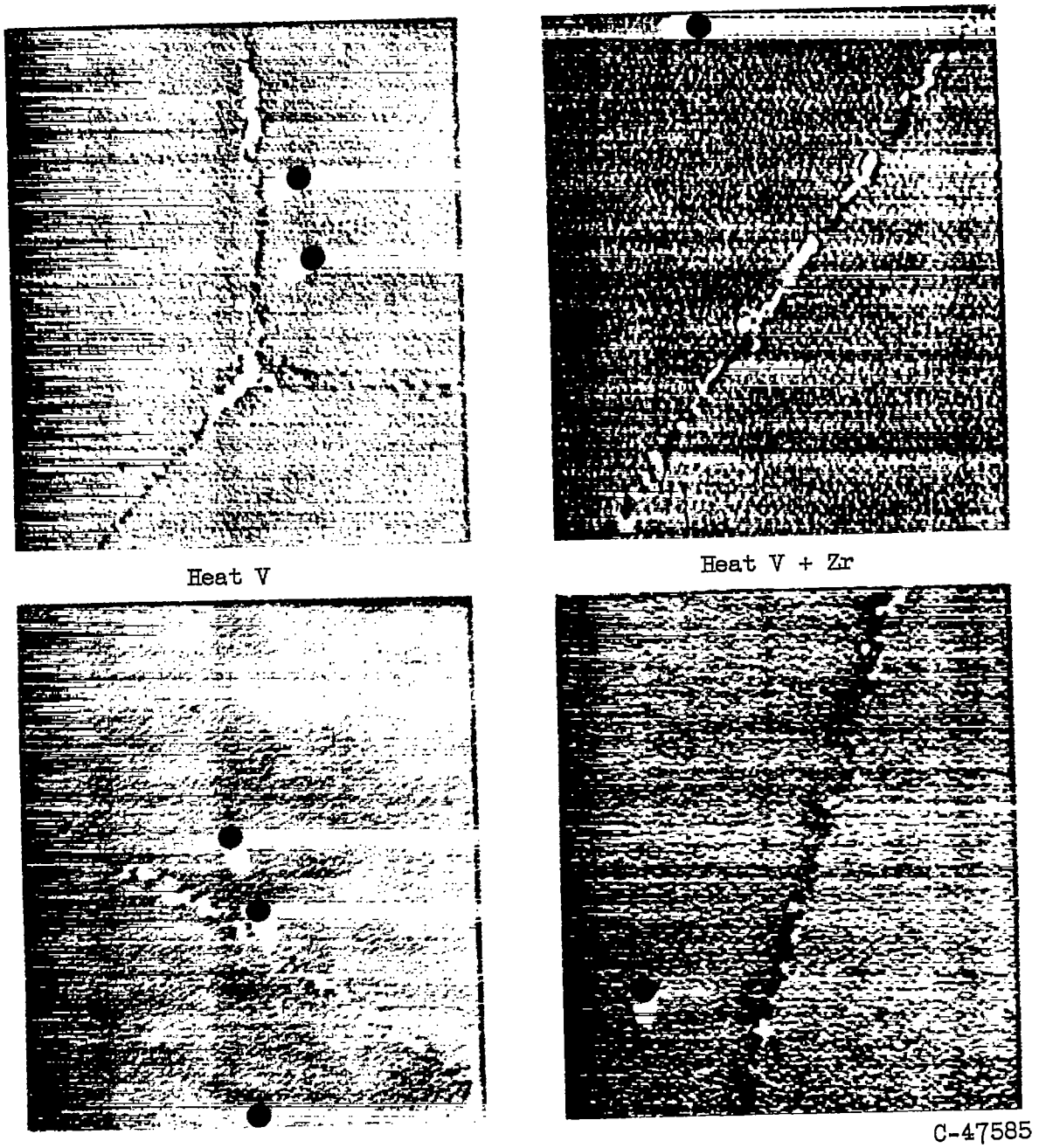

(c) Electron micrographs, X12,000.

Figure 6. - Concluded.

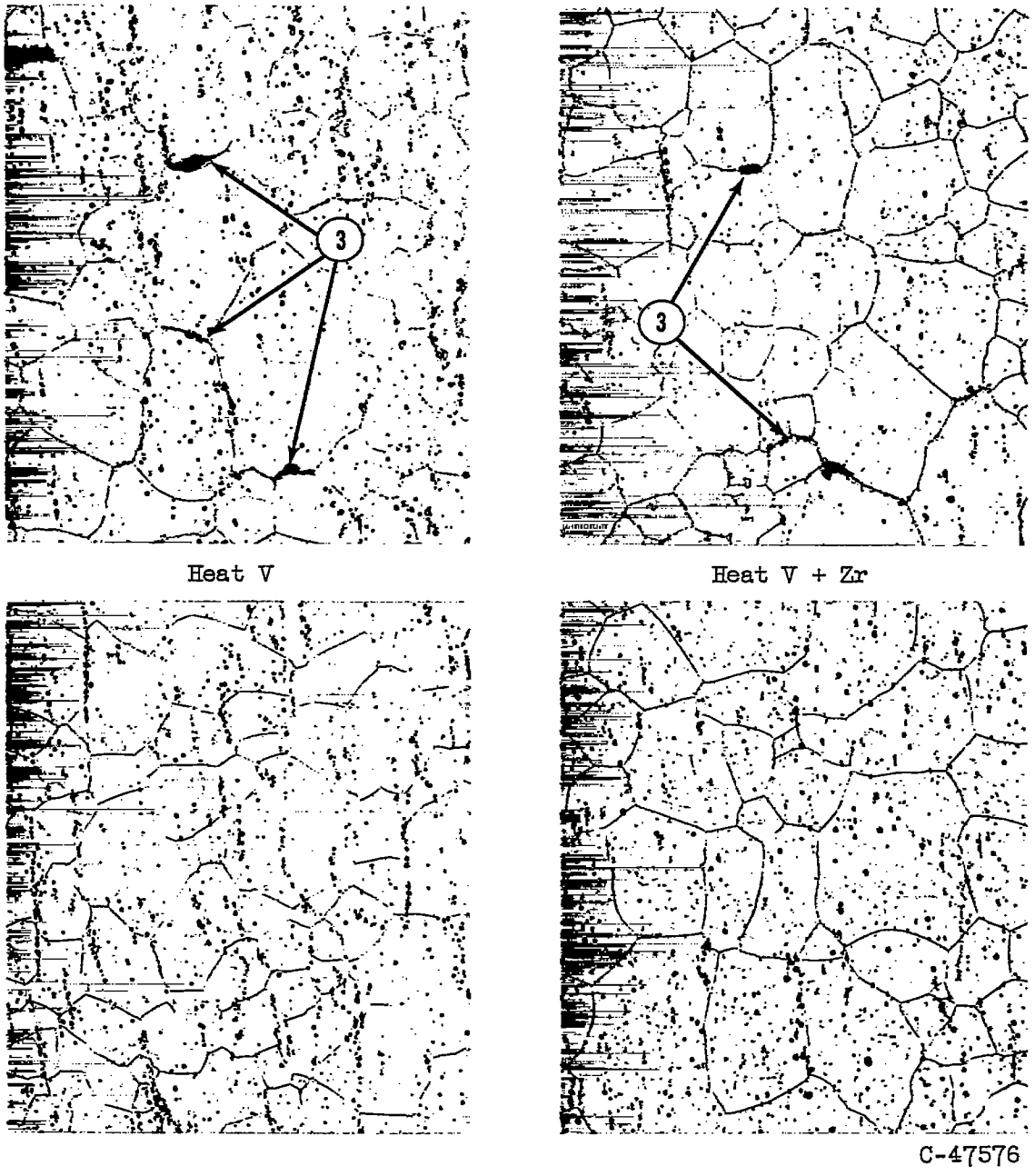

Heat V

Heat V + Zr

Heat V + B

Heat V + B + Zr

(a) Electropolished specimens, X100. ③ Micro-crack.

Figure 7. - Microstructures of experimental heats after 1.2-percent deformation by creep at 1,600° F in 165 to 214 hours.

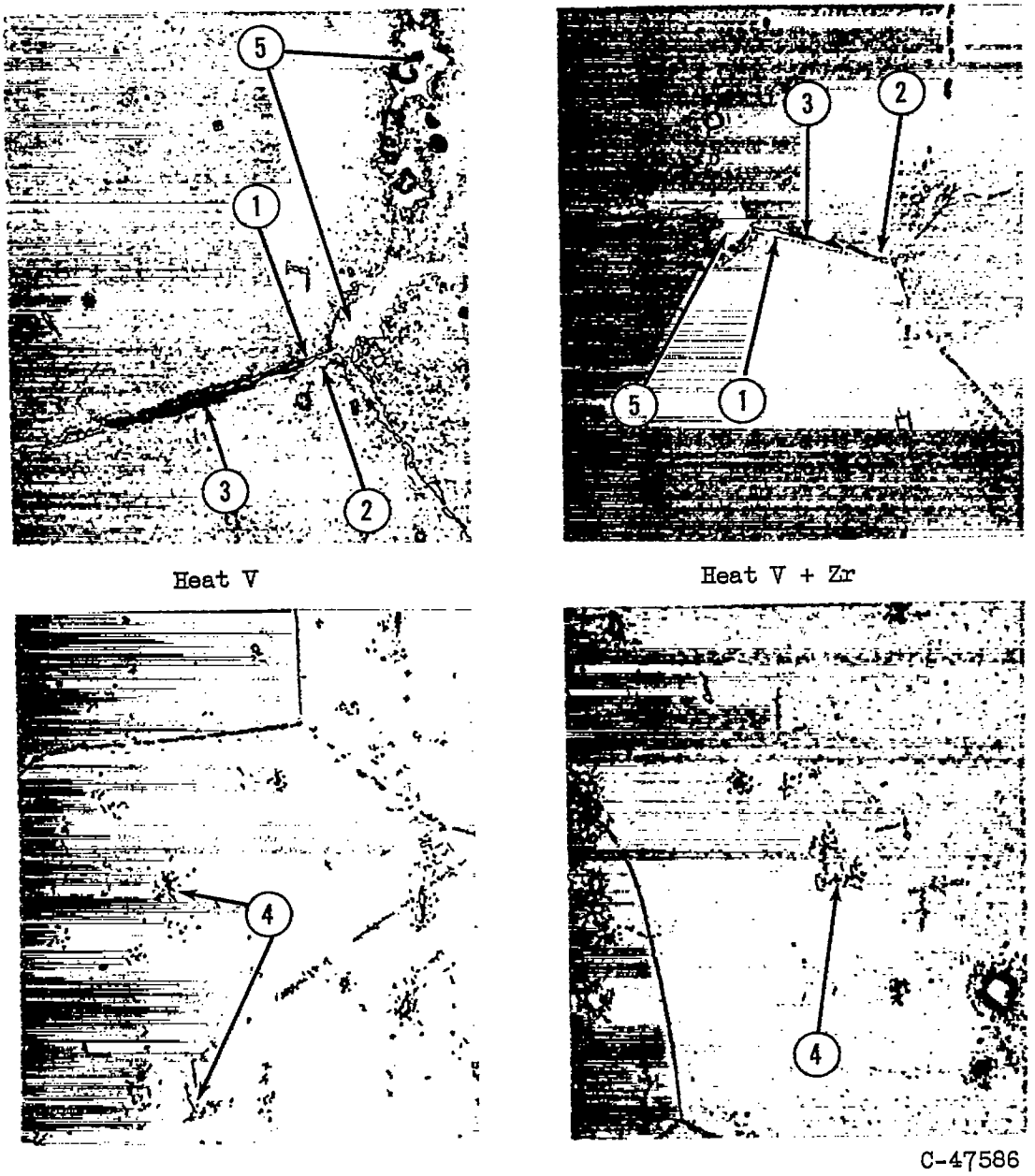

(b) Magnification, X1,000. ①Intergranular $M_{23}C_6$; ②depleted grain boundary; ③micro-crack; ④intragranular carbide; ⑤nodule.

Figure 7. - Continued.

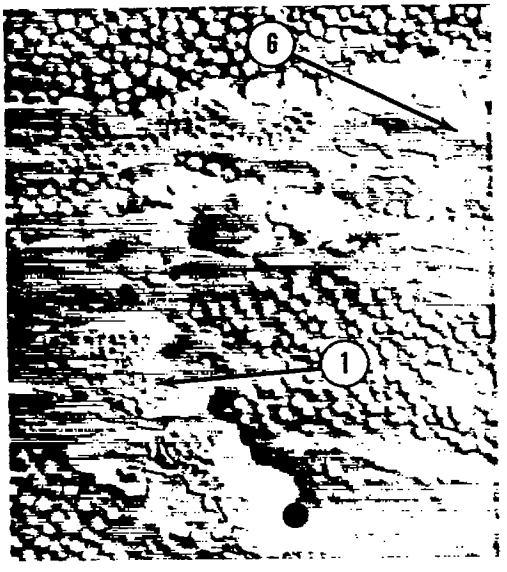

Heat V; typical grain boundaries

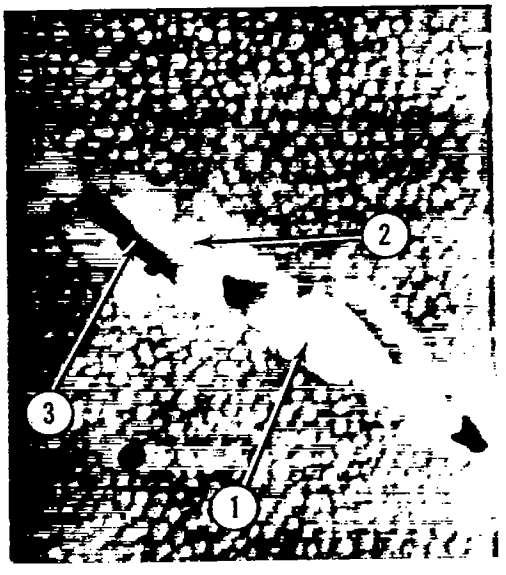

Heat V + Zr; depleted and cracked grain boundary with typical $M_{23}C_6$ precipitate

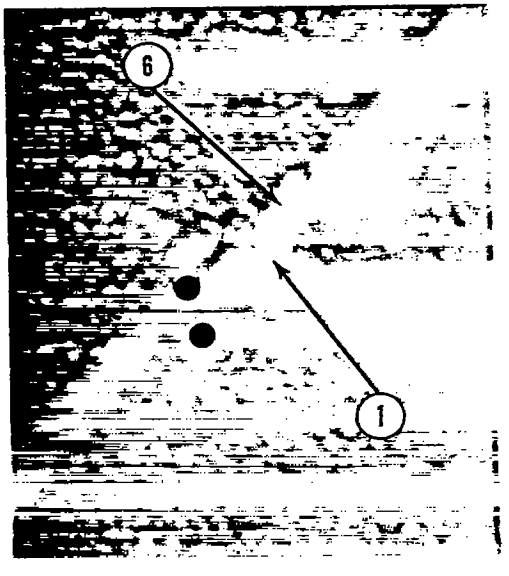

Heat V + B; typical grain boundary

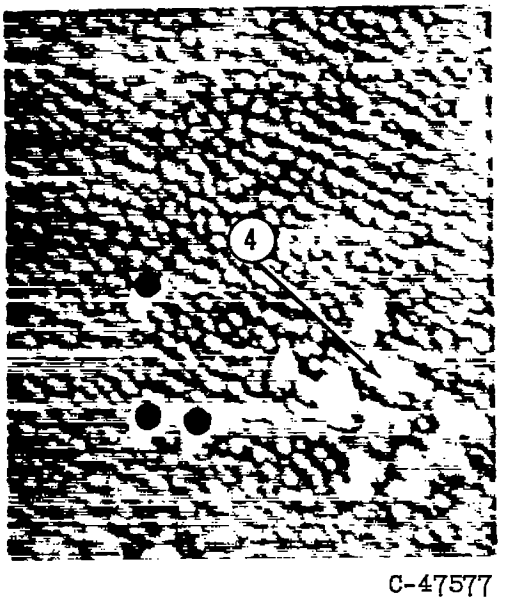

C-47577

Heat V + B; intragranular carbides and alinement of γ'

(c) Electron micrographs, X12,000. ①Intergranular $M_{23}C_6$; ②depleted grain boundary; ③micro-crack; ④intragranular carbide; ⑥γ'.

Figure 7. - Continued.

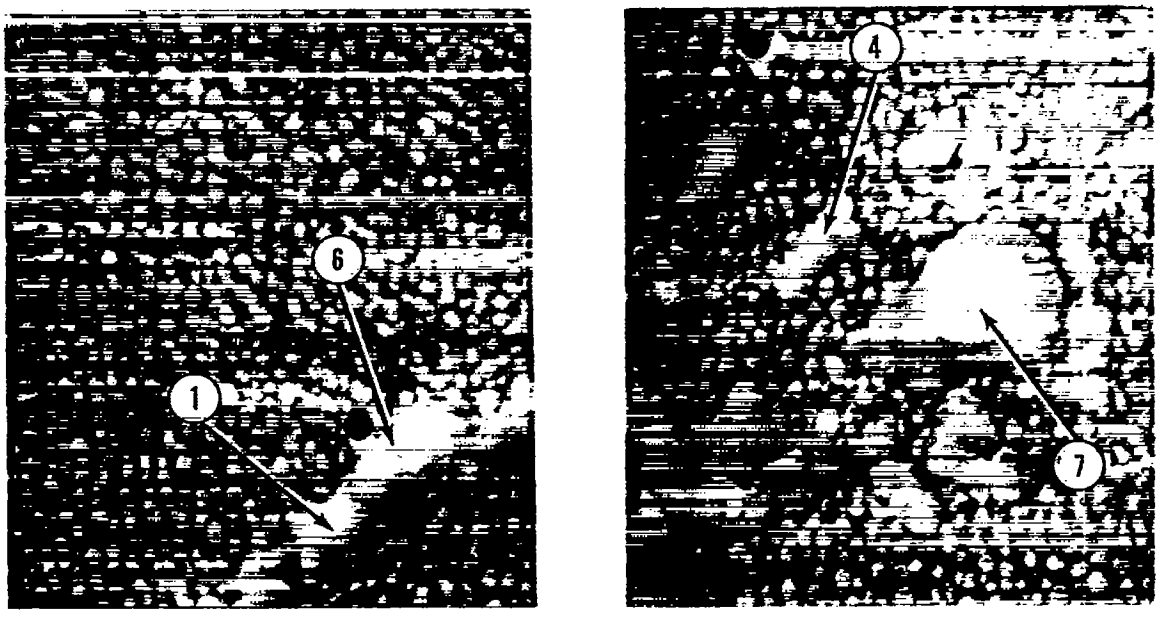

C-47578

Heat V + B + Zr; typical grain boundary and alinement of γ'

Heat V + B + Zr; intragranular carbides surrounding Ti(C,N)

(c) Concluded. ①Intergranular $M_{23}C_6$; ④intragranular carbide; ⑥γ'; ⑦Ti(C,N).

Figure 7. Concluded.

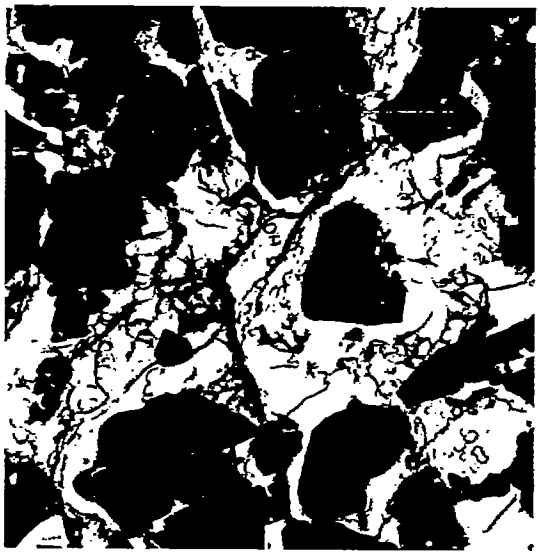

(a) Extraction replica of carbide from intergranular fracture surface of heat V after 1.2-percent creep deformation in 165 hours at 1,600° F. All selected area electron diffraction spots indexed as $M_{23}C_6$. Magnification, X8,000.

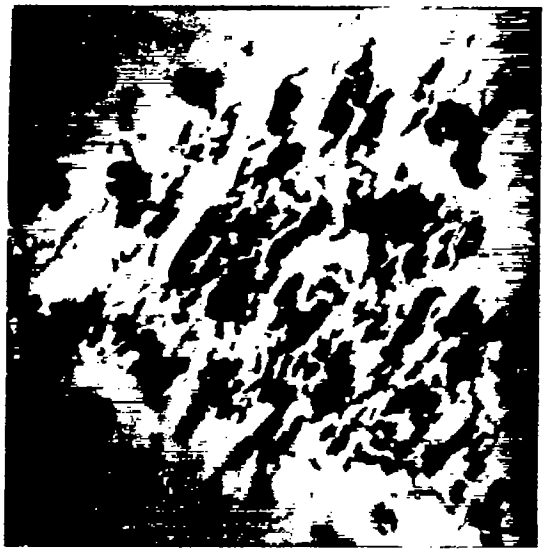

(b) Extraction replica of carbide from intergranular fracture surface of heat V + B after 1.2-percent creep deformation in 188 hours at 1,600° F. All selected area electron diffraction spots indexed as $M_{23}C_6$. Magnification, X8,000.

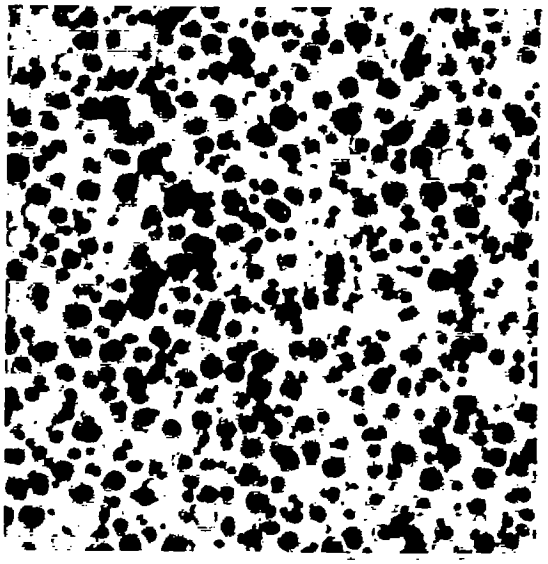

(c) Extraction replica of intragranular γ' from heat V + Zr after aging 10 hours at 1,600° F. All selected area electron diffraction spots indexed as γ'. Magnification, X36,000.

C-47587

(d) Extraction replica of intragranular carbide from heat V + B after 1.2-percent creep deformation in 188 hours at 1,600° F. Most selected area electron diffraction spots indexed as M_6C, a few as $M_{23}C_6$. Magnification, X8,000.

Figure 8. - Micrographs of phases extracted from experimental heats. Extracted particles appear black.

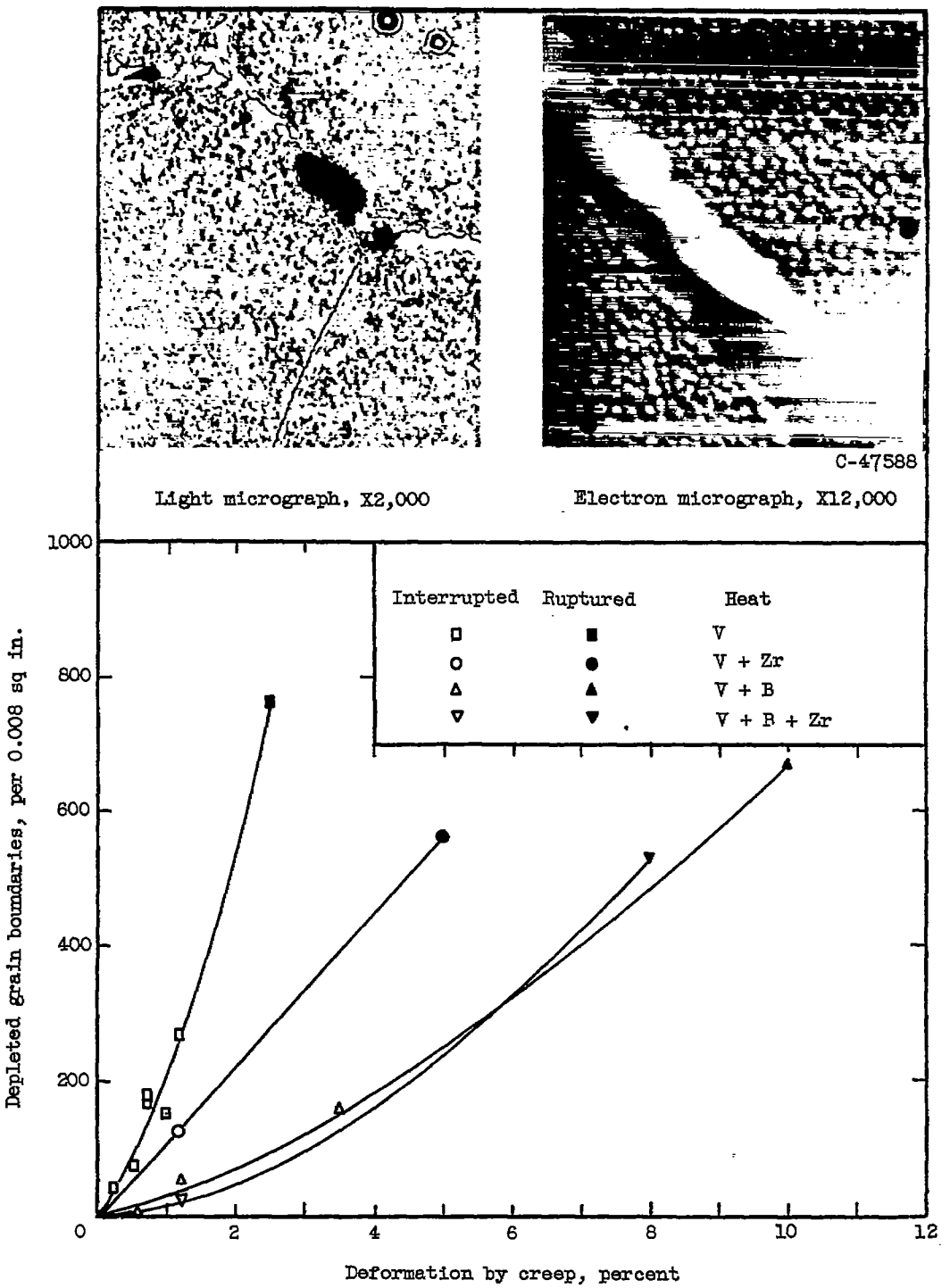

Figure 9. - Effect of creep deformation at 1,600° F on depletion of grain boundaries of experimental heats stressed to give comparable strain rates. Micrographs of typical depleted grain boundaries are shown for electropolished specimen.

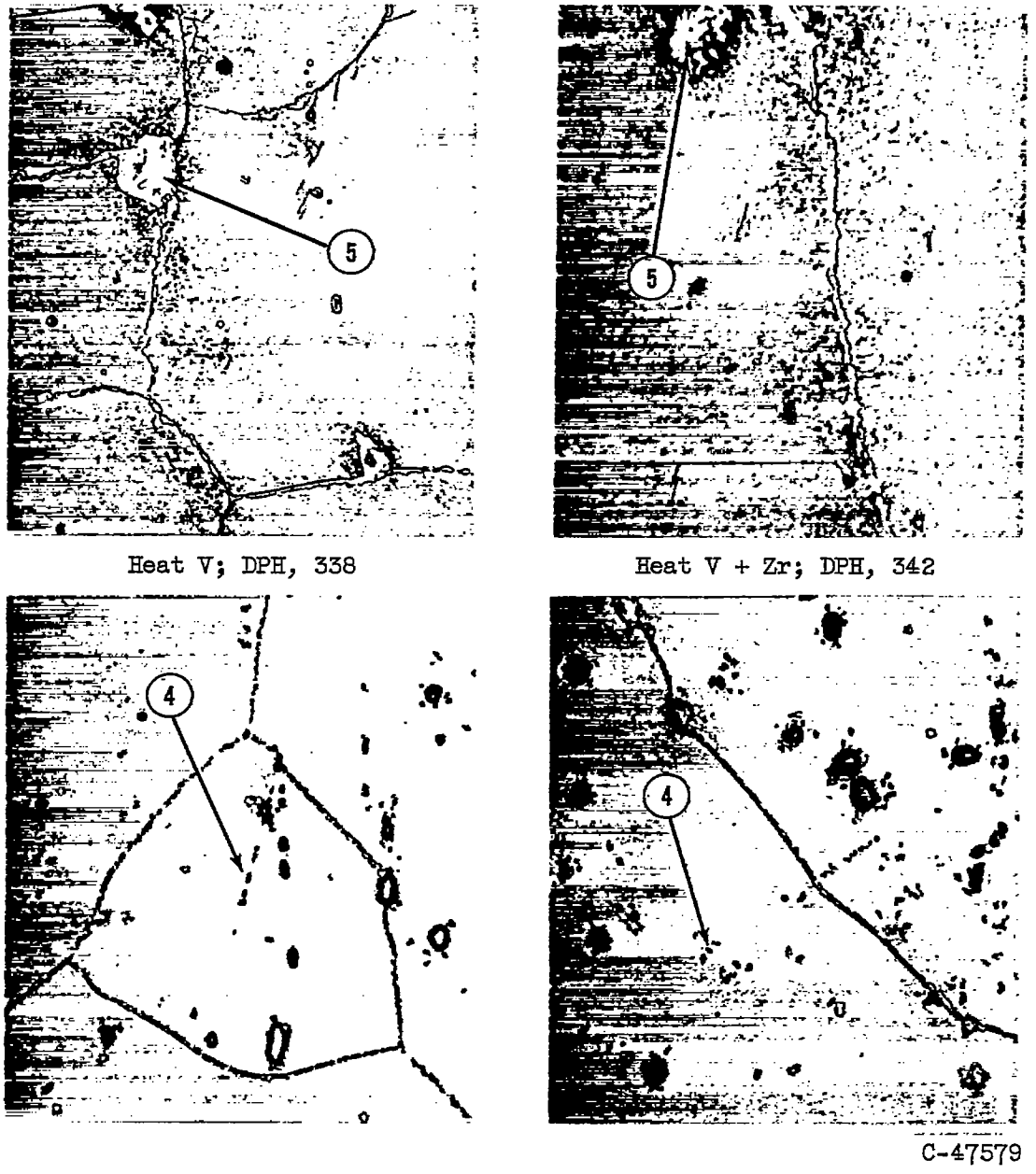

Heat V; DPH, 338

Heat V + Zr; DPH, 342

Heat V + B; DPH, 340

Heat V + B + Zr; DPH, 353

(a) Magnification, X1,000. ④Intragranular carbide; ⑤nodule.

Figure 10.- Microstructures of experimental heats after aging 188 hours at 1,600° F.

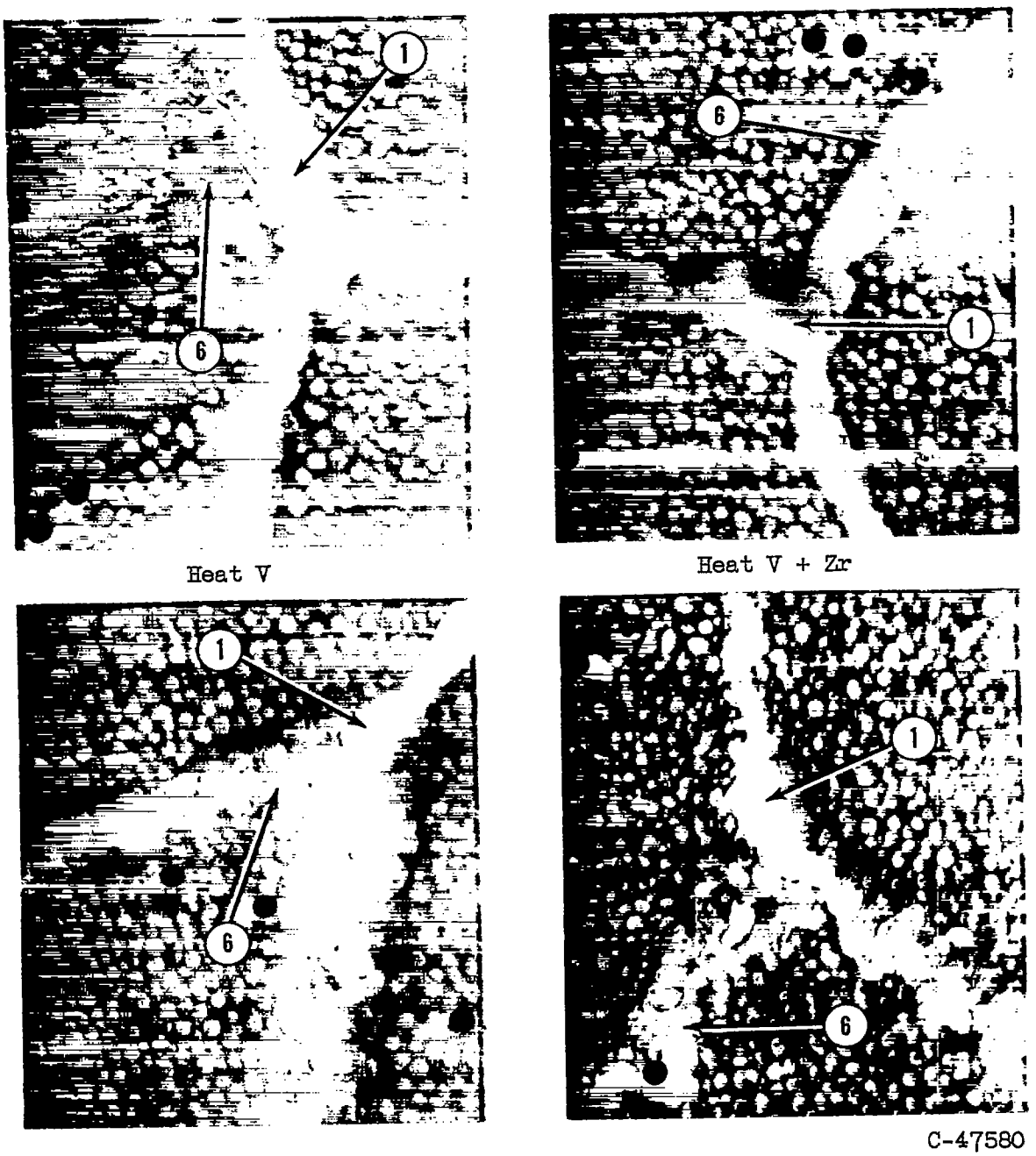

(b) Electron micrographs, X12,000. ①Intergranular $M_{23}C_6$; ⑥γ'.

Figure 10. - Concluded.

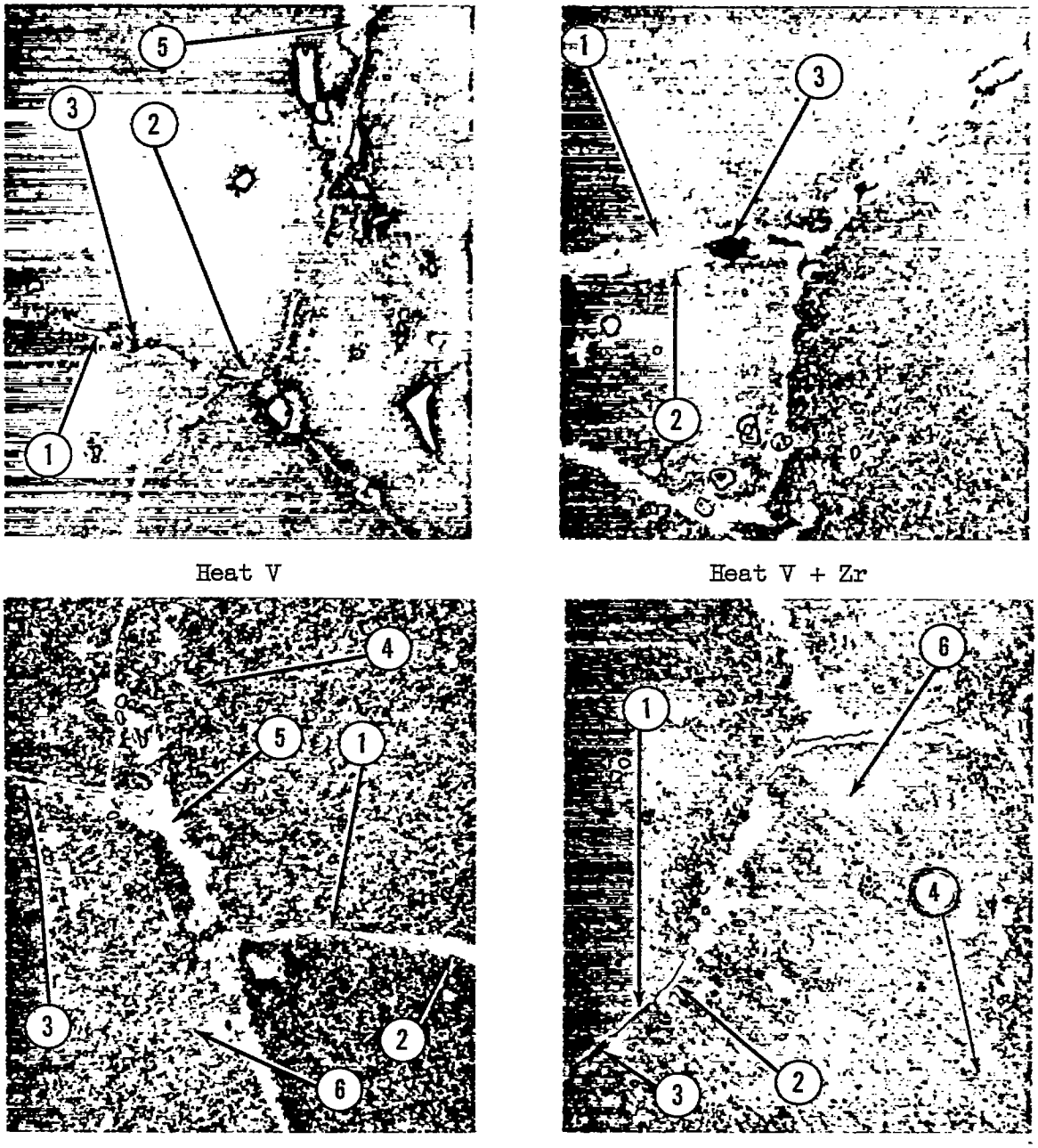

Figure 11. - Microstructures of experimental heats after rupture at 1,600° F and 25,000 psi. Magnification, X1,000 diameters. ① Intergranular $M_{23}C_6$; ② depleted grain boundary; ③ micro-crack; ④ intragranular carbide; ⑤ nodule; ⑥ alinement of γ'.

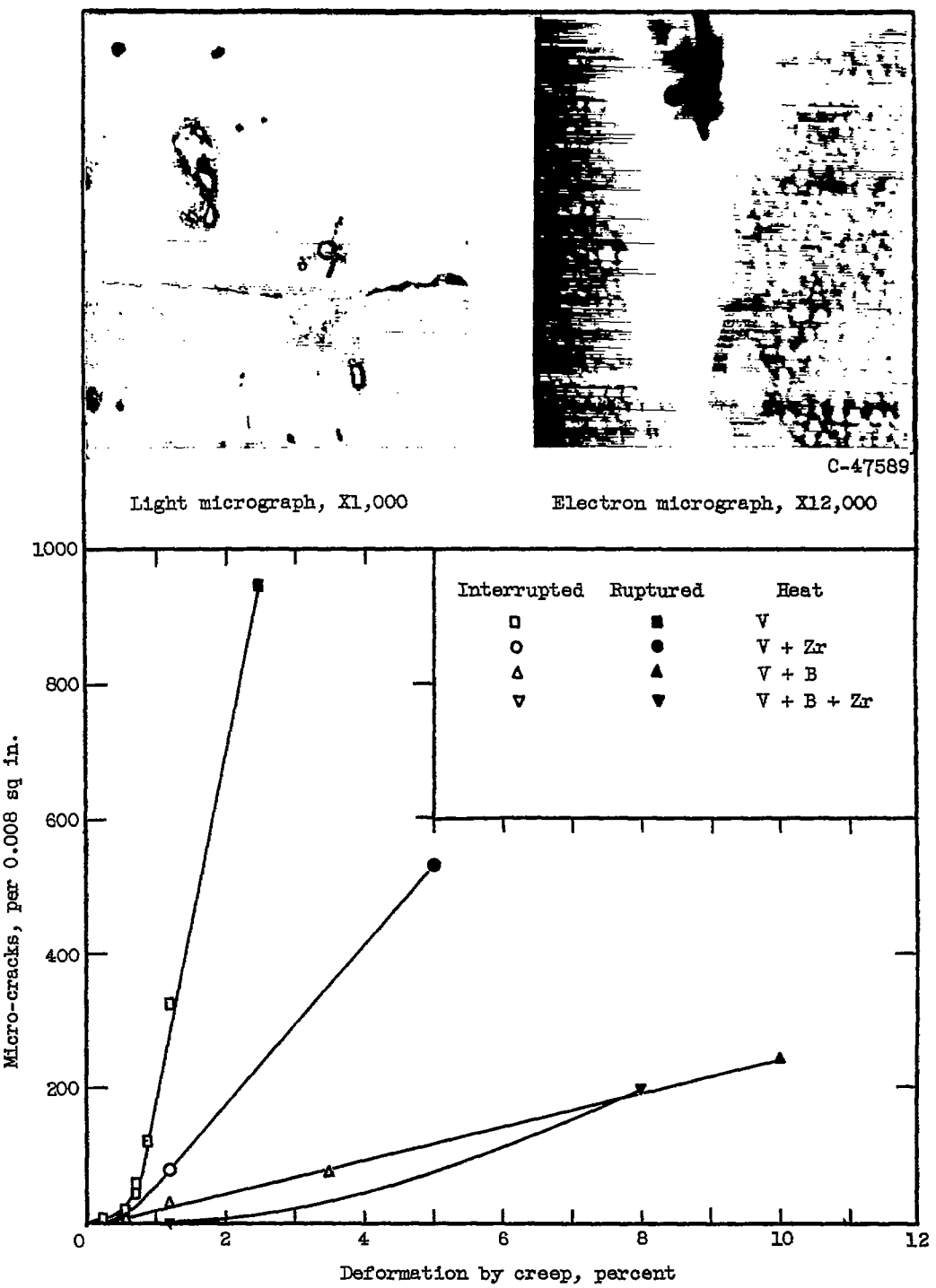

Figure 12.-- Effect of creep deformation at 1,600° F on micro-cracking of experimental heats. Stressed to give comparable strain rates. Micrographs of typical micro-cracks are shown. Tension axis is horizontal in the electron micrograph.

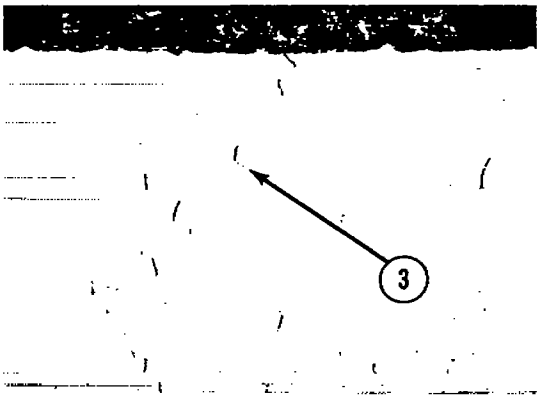

(a) Heat V, ruptured in 52 hours at 1,600° F and 25,000 psi with 13 surface cracks and 376 micro-cracks.

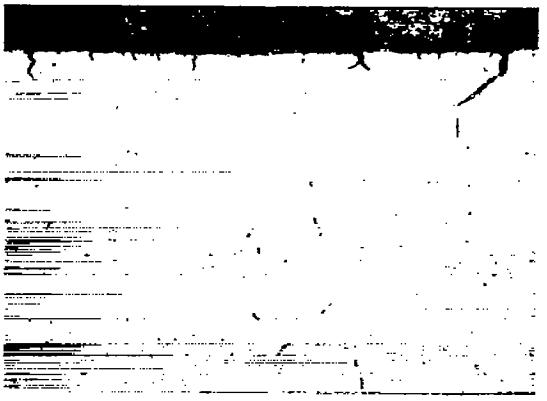

(b) Heat V + B, ruptured in 296 hours at 1,600° F and 28,000 psi with 160 surface cracks and 243 micro-cracks.

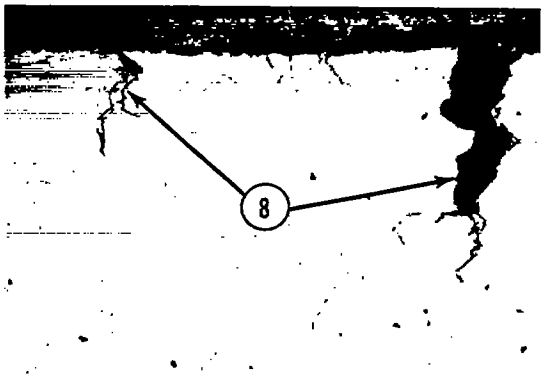

(c) Heat V + B + Zr, ruptured in 266 hours at 1,600° F and 30,000 psi with 300 surface cracks and 198 micro-cracks.

Figure 13. - Change in mode of cracking in experimental heats. Surface cracks are number per inch of transverse section penetrating more than 0.003 inch. Micro-cracks are number in 0.008 square inch observed. Magnification, X32. ③ Micro-crack; ⑧ surface cracks.

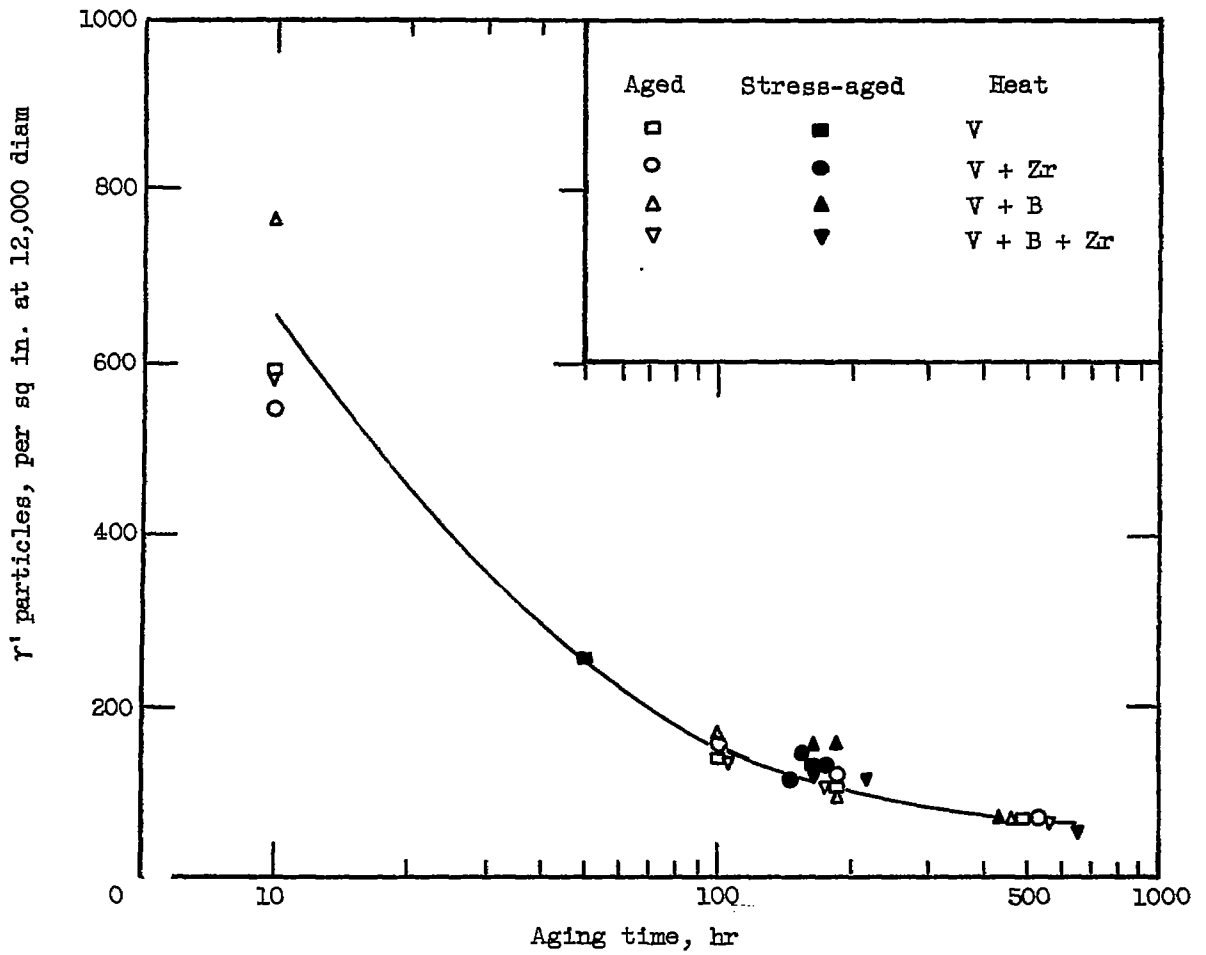

Figure 14. - Effect of aging time at 1,600° F on γ' particle density in experimental heats. Stress-aging was at 20,000 to 30,000 psi.

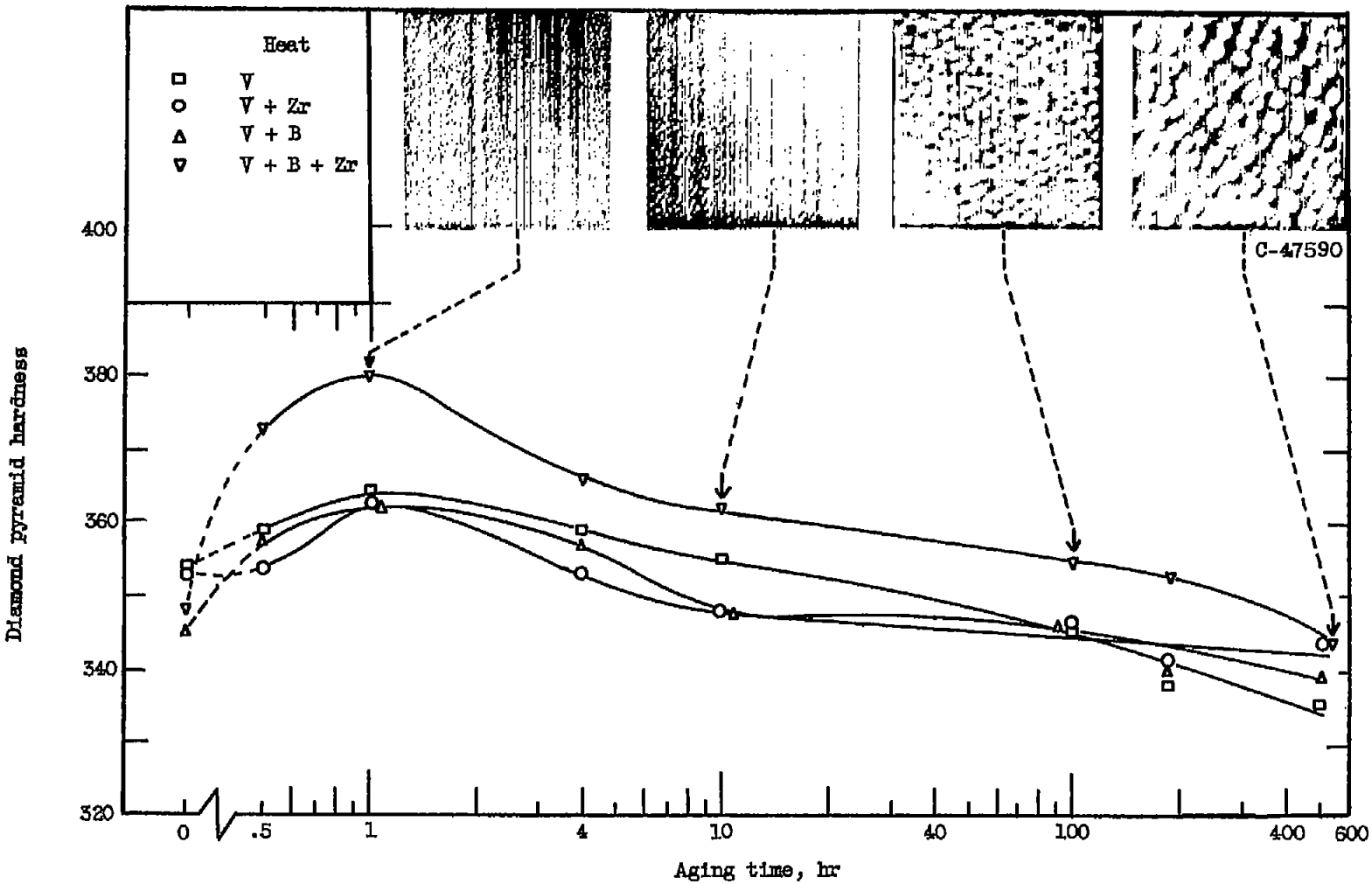

Figure 15. - Effect of aging at 1,600° F on hardness and γ' dispersion of experimental heats. Typical electron micrographs at 12,000 diameters are shown.

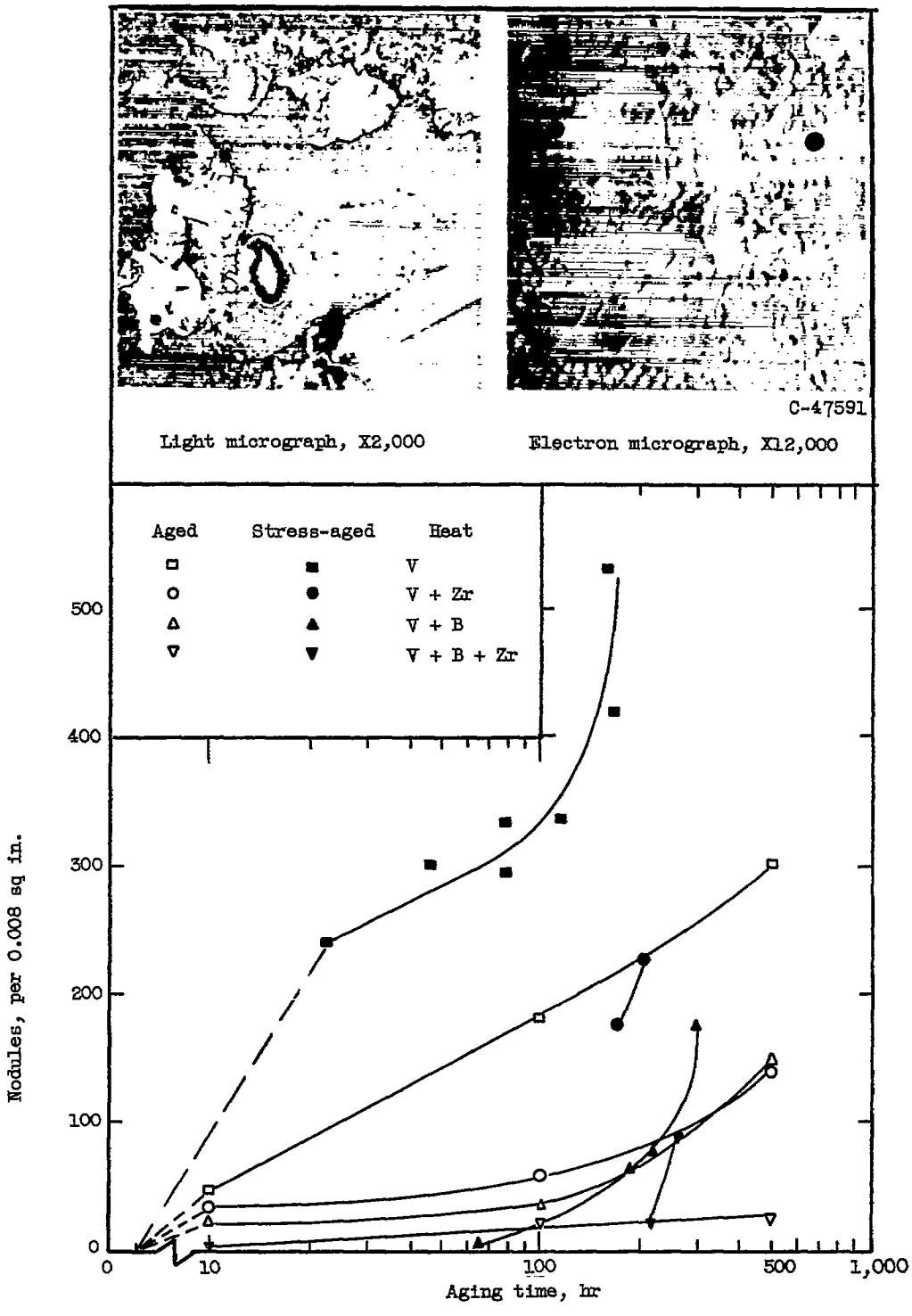

Figure 16. - Effect of aging time at 1,600° F on nodule density of experimental heats. Stress-aging was at comparable strain rates. Micrographs of typical nodules are shown.

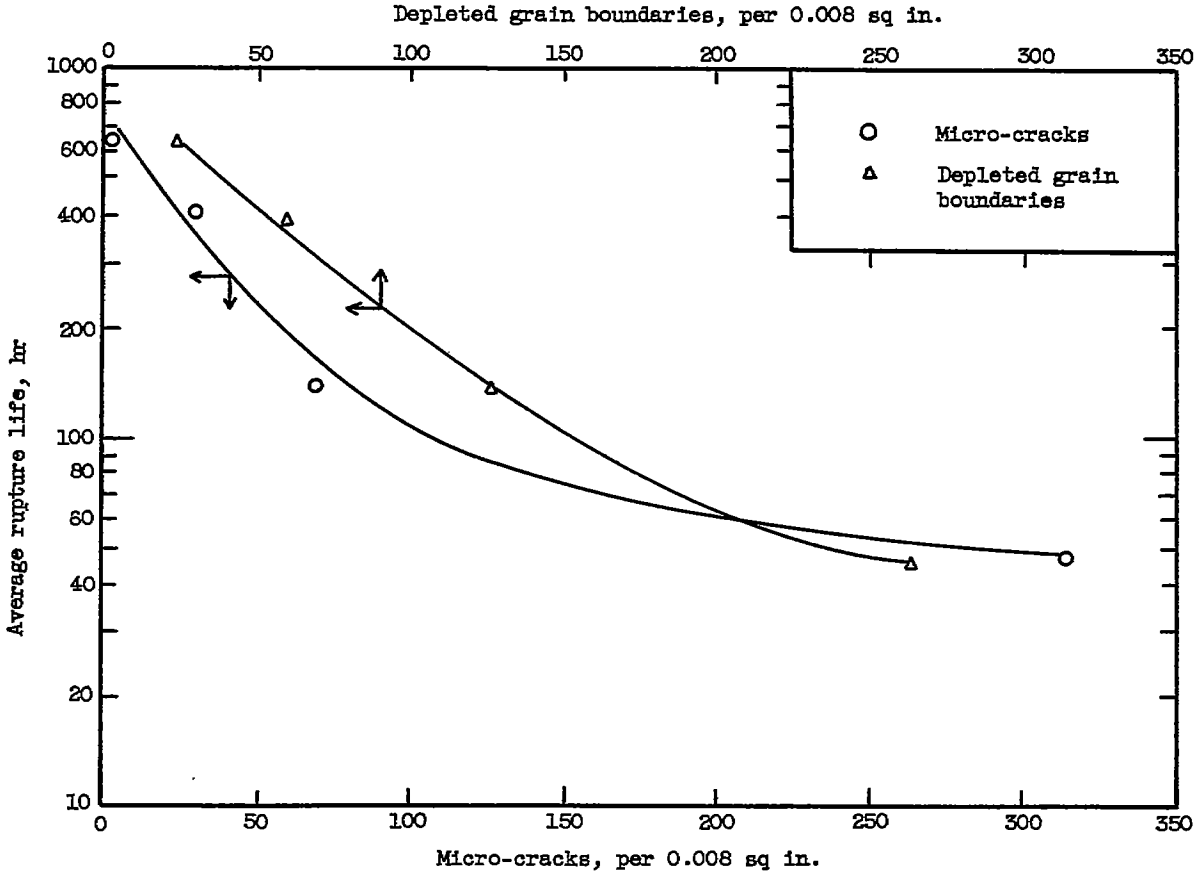

Figure 17. - Relation of rupture life at 1,600° F and 25,000 psi to micro-cracking and depletion tendencies of experimental heats when stressed to give 1.2-percent deformation in 165 to 214 hours.

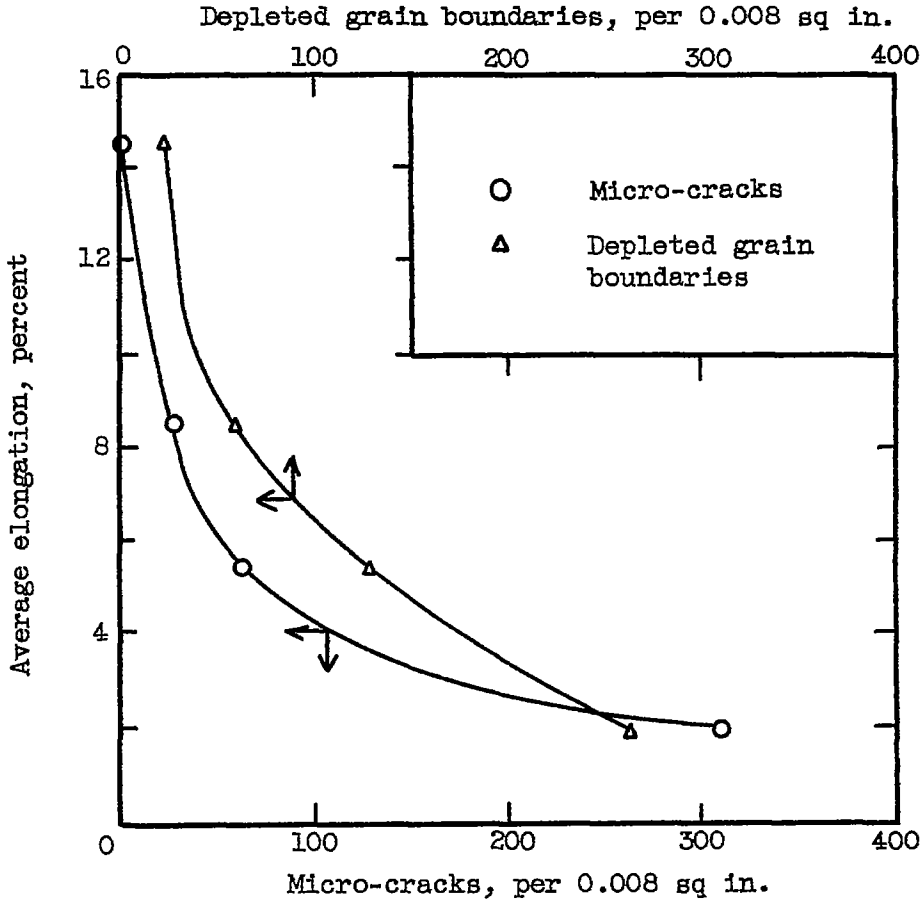

Figure 18. - Relation of elongation at 1,600° F and 25,000 psi to micro-cracking and depletion tendencies of experimental heats when stressed to give 1.2-percent deformation in 165 to 214 hours.